

Structure Design and Processing Strategies of MXene-Based Materials for Electromagnetic Interference Shielding

Oliveira, Filipa M.; Azadmanjiri, Jalal; Wang, Xuehang; Yu, Minghao; Sofer, Zdeněk

DOI

[10.1002/smt.202300112](https://doi.org/10.1002/smt.202300112)

Publication date

2023

Document Version

Final published version

Published in

SMALL METHODS

Citation (APA)

Oliveira, F. M., Azadmanjiri, J., Wang, X., Yu, M., & Sofer, Z. (2023). Structure Design and Processing Strategies of MXene-Based Materials for Electromagnetic Interference Shielding. *SMALL METHODS*, 7(7), Article 2300112. <https://doi.org/10.1002/smt.202300112>

Important note

To cite this publication, please use the final published version (if applicable). Please check the document version above.

Copyright

Other than for strictly personal use, it is not permitted to download, forward or distribute the text or part of it, without the consent of the author(s) and/or copyright holder(s), unless the work is under an open content license such as Creative Commons.

Takedown policy

Please contact us and provide details if you believe this document breaches copyrights. We will remove access to the work immediately and investigate your claim.

Structure Design and Processing Strategies of MXene-Based Materials for Electromagnetic Interference Shielding

Filipa M. Oliveira,* Jalal Azadmanjiri, Xuehang Wang, Minghao Yu, and Zdeněk Sofer*

The development of new materials for electromagnetic interference (EMI) shielding is an important area of research, as it allows for the creation of more effective and high-efficient shielding solutions. In this sense, MXenes, a class of 2D transition metal carbides and nitrides have exhibited promising performances as EMI shielding materials. Electric conductivity, low density, and flexibility are some of the properties given by MXene materials, which make them very attractive in the field. Different processing techniques have been employed to produce MXene-based materials with EMI shielding properties. This review summarizes processes and the role of key parameters like the content of fillers and thickness in the desired EMI shielding performance. It also discusses the determination of power coefficients in defining the EMI shielding mechanism and the concept of green shielding materials, as well as their influence on the real application of a produced material. The review concludes with a summary of current challenges and prospects in the production of MXene materials as EMI shields.

EMI shielding could be considered a critical aspect of modern technology which helps to protect electronic devices from external sources of interference that can disrupt their normal functioning. This interference can come from a variety of sources such as other electronic devices, power lines, and even natural phenomena like lightning. Without effective EMI shielding, electronic devices can suffer from a range of problems including reduced performance, data loss, and even physical damage. Harmful effects on the health of human beings are also a matter of concern that could be caused by electromagnetic waves (EMW) in the environment.^[1-4] The development of new materials for EMI shielding is thus an important area of research as it allows for the potential production of effective and efficient EMI shielding solutions.

1. Introduction


The development of high-frequency circuits and wireless communication devices in industrial and high-technology applications, as well as the rapid progress in the number of radio-frequency radiation sources have resulted in electromagnetic interference (EMI) attracting a significant value of attention. Thus,

A material is evaluated to be shielded if the material is sufficiently electrically conductive to shield against influence from an outside electromagnetic wave. Hence, the most common materials used for EMI shielding applications are metals such as copper, aluminum, or stainless steel, to name a few, due to their high conductivity and ability to block EMW. However, there are some limitations for metals as a category of materials for EMI shielding such as their considerable weight, physical rigidity, and susceptibility to corrosion. These characteristics of the metals make them difficult to be used in devices where flexibility, low weight, or high resistivity to corrosion are important.^[1,3] Additionally, metals are expensive and may not be the most cost-effective option in some cases. Other materials, such as intrinsic conductive polymers (ICP) or polymer composites which result from a combination of an insulator polymer matrix with conductive and/or magnetic fillers, can be molded into complex shapes and are often used in EMI shielding applications where flexibility is important. However, ICP and polymer composites generally are susceptible to degradation over time, especially when exposed to high temperatures or harsh environmental conditions.^[5,6] This can limit their durability and lifespan and may make them less suitable for certain applications. High electrically conductive coatings and inks are another category of materials that can be considered for EMI shielding.^[7,8] Albeit, they also can be difficult to apply evenly and consistently and may require specialized equipment. It is thus clear that common factors that influence the choice of a material to produce an efficient EMI shield include conductivity, flexibility, durability, and cost.

F. M. Oliveira, J. Azadmanjiri, Z. Sofer
Department of Inorganic Chemistry
Faculty of Chemical Technology
University of Chemistry and Technology Prague
Prague 6, 166 28, Czech Republic
E-mail: filipa.oliveira@vscht.cz; zdenek.sofer@vscht.cz

X. Wang
Department of Radiation Science and Technology
Faculty of Applied Sciences
Delft University of Technology
Delft 2629JB, The Netherlands

M. Yu
Centre for Advancing Electronics Dresden (cfaed) & Faculty of Chemistry and Food Chemistry
Technische Universität Dresden
01062 Dresden, Germany

 The ORCID identification number(s) for the author(s) of this article can be found under <https://doi.org/10.1002/smt.202300112>

© 2023 The Authors. Small Methods published by Wiley-VCH GmbH. This is an open access article under the terms of the Creative Commons Attribution License, which permits use, distribution and reproduction in any medium, provided the original work is properly cited.

DOI: 10.1002/smt.202300112

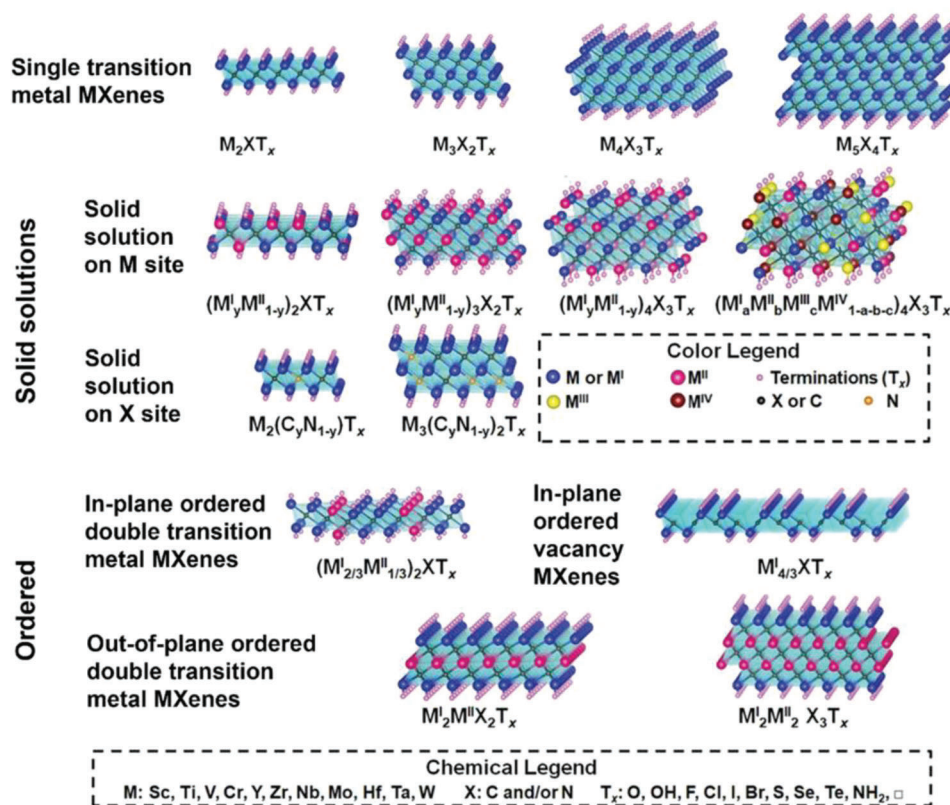


Figure 1. Typical MXene structures and compositions. Reproduced with permission.^[22] Copyright 2021, Wiley-VCH.

To meet the above-mentioned prerequisites, transition metal carbides and nitrides, mostly known as MXenes, have been suggested as potential EMI shields.^[9–12] This class of 2D materials was reported for the first time by researchers from Drexel University in 2011 with the synthesis of $\text{Ti}_3\text{C}_2\text{T}_x$.^[13] MXenes are made from a class of materials known as MAX phases, which are a combination of metal and a chemically-bound carbon or nitrogen layer. MAX phases have $\text{M}_{n+1}\text{AX}_n$ as a general formula, where M is a transition metal, A is an A-group element (mostly group 13 and 14 elements of the periodic table), X is carbon and/or nitrogen, and $n = 1–4$ indicates the number of M layers separating the A layers.^[14,15] The MAX phases combine the best characteristics of metals, such as good electrical and thermal conductivity and magnetic properties, with high elastic moduli, temperature resistance, and resistance to oxidation and corrosion of ceramics.^[16]

By selective etching of the A-group element, MXene materials with 2D layered structures and unique properties are created that are promising materials for many applications.^[4,17–19] This selective etching is a key step in the synthesis of MXenes materials and should be carefully controlled to ensure that only the A-group element is removed, as the properties of the MXene are largely determined by the selected transition metal (M). With these etching processes, the surfaces of MXenes are terminated by functional groups (T_x), such as $-\text{O}$, $-\text{OH}$, $-\text{F}$, or $-\text{Cl}$, resulting in a general formula of $\text{M}_{n+1}\text{X}_n\text{T}_x$ (Figure 1).^[20–22] The presence of these terminal groups can influence the performance of the MXenes in different ways, including their EMI shielding properties. Because terminal groups represent defects on the MXenes sur-

face which enhances polarization losses, making them more effective in absorbing EMW and converting their energy into other forms like thermal energy. The current etching routes of MAX phases include aqueous acid etching in hydrofluoric acid (HF) containing solution, molten salt etching and Lewis acidic molten salt etching, alkali etching, electrochemical etching, and ionic liquid-based etching routes.^[15,23] Moreover, MXenes can be classified into different categories based on their atomic lattices and compositions: ordered mono-M, ordered double-M, and solid-solution M elements (Figure 1).^[22] More recently, high-entropy MXenes with four or more M elements have enriched the MXenes family.^[24–27]

Hence, MXenes have great potential as EMI shielding because of their unique properties: they are electrically conductive, which is a key requirement for effective EMI shielding; MXenes are corrosion-resistant, which means that they can be used in harsh environments without losing their effectiveness as a shielding material; MXenes are flexible and lightweight, which makes them well-suited for use in applications where these characteristics are important, like wearable devices or other applications where the EMI shield needs to be molded or shaped to fit a specific geometry, or where weight is a critical factor.

Numerous results have been achieved on the EMI shielding properties of MXenes and compiled in many literature reviews, providing valuable information about the potential of MXenes as EMI shieldings. However, they are mostly focused on the MXene performance and often do not address the processing techniques and how they play an important role in optimizing the structure

and performance of MXene materials and their composites. The selection of a certain processing technique may influence parameters like the total amount of MXene and other fillers included in the final product, thickness, and potential chemical modifications. By carefully controlling these parameters, it is possible to fine-tune the properties of the final product in order to improve its performance and effectiveness as an EMI shielding.

Therefore, this review addresses the different processing techniques that have been used in the production of MXene materials with EMI shielding properties and their role in architecting different structures for a significant impact in this field. Furthermore, in recent years and based on concerns associated with EM pollution, the concept of green shielding material has attracted the attention of researchers on the development of EMI shielding materials.^[28–30] Hence, this review also emphasizes current progress on MXene-based materials with a favorable green shielding index (g_s) for the environment along with the challenges involved in their production, being thus the first review focused only on MXenes that discuss this matter of concern. Finally, challenges and research perspectives on the current processing techniques which are used for producing EMI shielding MXene-based materials, in particular considering scalable manufacturing in industry, are discussed.

2. Electromagnetic Interference Shielding

2.1. Shielding Effectiveness and Its Mechanisms

EMI shielding is a process of attenuating and limiting the flow of EM fields between two locations by reflection (R), absorption (A), and/or multiple (M) mechanisms of EMW using a shielding material against the penetration of incoming radiation. The primary mechanism for EMI shielding is reflection. This occurs due to the impedance discrepancy between air and the material subjected to EMI. Materials used for reflection shielding comprise mobile charge carriers that interact with the EM field and reflect or attenuate the radiation. The second shielding mechanism is absorption. This happens due to power dissipation, while EM waves interact with the electric and/or magnetic dipoles of the material. A material with a reflection shielding mechanism prevents EM radiation transmission by its reflecting, while an absorption shielding material prevents EM radiation transmission by its absorbing and dissipation. Thus, very conductive materials are responsible for reflecting EMW, while magnetic or dielectric materials are characteristic of the absorption mechanism. The total of such attenuations can be quantified and it is called shielding effectiveness (SE) of a shielding material equals the sum of the reflection factor (SE_R), the absorption factor (SE_A), and the correction factor to account for multiple reflections (SE_M). Therefore, the SE can be written as^[31]

$$SE = SE_R + SE_A + SE_M \quad (1)$$

If the EM shielding is evaluated in terms of attenuation of the electric (E) or magnetic (H) field, the expression for SE is

$$SE = 20 \log \left(\frac{E_0}{E_1} \right) = 20 \log \left(\frac{H_0}{H_1} \right) \quad (2)$$

where E_0, H_0 is the intensity of the incident field, and E_1, H_1 is the intensity of the transmitted EMW. The shielding unit is determined in decibels (dB) because it expresses the ratio of field intensity in the absence (E_0, H_0) and presence (E_1, H_1) of the shield; and it is a logarithmic expression as the dB comes from the logarithmic unit *bel* which is defined as a power ratio of 10, allowing it to cover a large dynamic range.^[31,32]

2.1.1. Reflection

Reflection is the primary mechanism of EMI shielding because, wherever a boundary between two materials occurs, the reflection of EMW will always occur.^[32] Hence, the reflection losses (SE_R) depend on the impedance mismatch between free space (Z_1) and the shield (Z_2), **Figure 2a**, and this difference in impedance can be written as^[31]

$$E_1 = \frac{2Z_2}{Z_1 + Z_2} E_0 \quad (3)$$

and for a magnetic field

$$H_1 = \frac{2Z_2}{Z_1 + Z_2} H_0 \quad (4)$$

where E_0, H_0 is the intensity of the incident wave and E_1, H_1 is the intensity of the transmitted EMW.

As the EMW will encounter a new boundary (**Figure 2b**), the intensity of the transmitted wave (E_t, H_t) through this second boundary is given by the following

$$E_t = \frac{2Z_2}{Z_1 + Z_2} E_1 \quad (5)$$

and

$$H_t = \frac{2Z_2}{Z_1 + Z_2} H_1 \quad (6)$$

Considering the determination of E_t and H_t as a function of the intensity of the incident waves (E_0, H_0), Equations (5) and (6) can be written as follows

$$E_t = \frac{4Z_1 Z_2}{Z_1 + Z_2^2} E_0 \quad (7)$$

and

$$H_t = \frac{4Z_1 Z_2}{Z_1 + Z_2^2} H_0 \quad (8)$$

Given that the shield is a conductor and the free space an insulator, $Z_1 \gg Z_2$. Thus, in an electric field (E), most of the reflection occurs at the first boundary while in a magnetic field (H) it takes place when the EMW comes across the second surface. Therefore, Equations (7) and (8) are simplified to

$$E_t = \frac{4Z_2}{Z_1} E_0 \quad (9)$$

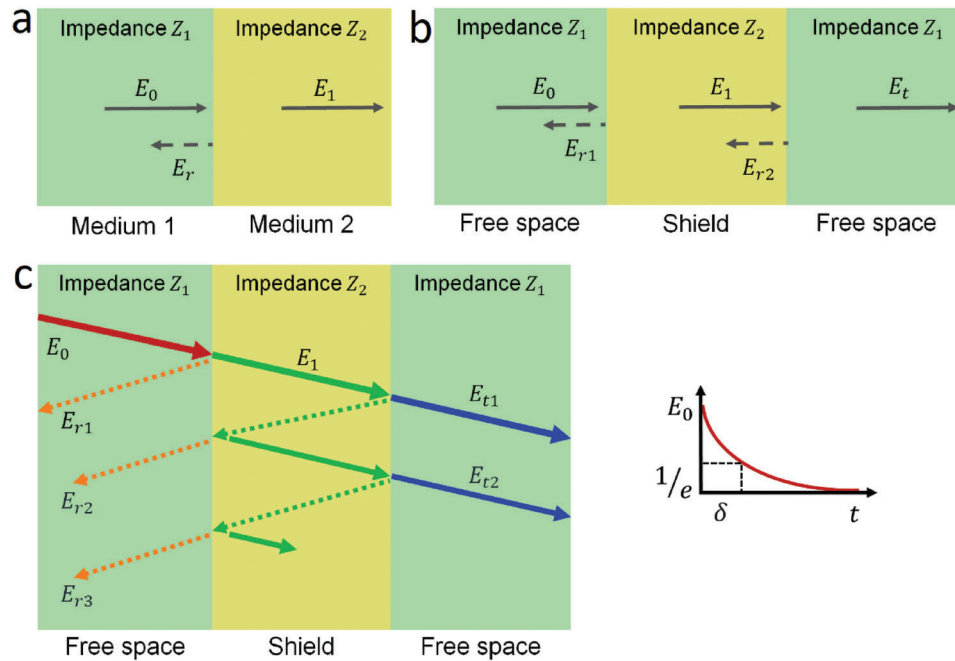


Figure 2. a) Illustration of the interaction of EMW in two different media: incident E_0 , transmitted E_1 , and reflected E_r EMW. b) Illustration of the interaction of EMW at the boundaries of a shield: E_0 is the incident EMW, E_1 is the transmitted EMW through the first boundary, and E_t is the total transmitted EMW. The reflection on boundaries is E_r (E_{r1} and E_{r2}). c) Illustration of the interaction of EMW in a shield: the incident E_0 EMW is transmitted through the first boundary (E_1), and can be transmitted (E_t) at each reflection, thus the multiple reflections. The inset shows the exponential attenuation of an EMW passing through a shield and respective skin depth (δ). Adapted with permission.^[31] Copyright 2009, Wiley-VCH.

and

$$H_t = \frac{4Z_2}{Z_1} H_0 \quad (10)$$

Finally, considering that Z_1 is the impedance of the EMW (Z_w) and Z_2 is the impedance of the shield (Z_s), the SE_R is determined as follows^[31]

$$SE_R = 20 \log \frac{E_0}{E_1} = 20 \log \frac{H_0}{H_1} = 20 \log \frac{Z_1}{4Z_2} = 20 \log \frac{|Z_w|}{4|Z_s|} \quad (11)$$

where

$$Z_w = \frac{E}{H} \quad (12)$$

and

$$|Z_s| = 3.68 \times 10^{-7} \sqrt{\frac{\mu_r}{\sigma_r}} \sqrt{f} \quad (13)$$

2.1.2. Absorption

The absorption mechanism of EMI shielding is happening when the nonreflected EMWs pass through the shield and their amplitudes decrease exponentially because currents induced in the shield produce ohmic losses and heating of the material. Therefore,

$$E_1 = E_0 e^{-t/\delta} \quad (14)$$

and

$$H_1 = H_0 e^{-t/\delta} \quad (15)$$

where E_1 and H_1 are the electric and magnetic fields, respectively, at a distance (or thickness) t .^[31] The intensity of the EMW is attenuated to 37% or $1/e$ (e is the Euler's number, $e = 2.71828$) of its initial value at a certain distance and that distance is defined as the skin depth (δ), which is written as

$$\delta = \sqrt{\frac{2}{f\mu\sigma}} \quad (16)$$

The absorption loss (SE_A) can be then determined by^[31]

$$SE_A = 20 \log \frac{E_0}{E_1} = 20 \log e^{t/\delta} = 20 \left(\frac{t}{\delta}\right) \log(e) = 8.69 \left(\frac{t}{\delta}\right) \quad (17)$$

It is clear that electric conductivity σ and magnetic permeability μ have a substantial role in the absorption capability of the shield, and that the skin depth is an important factor when defining the thickness of the shield since a thicker shield may result in excessive cost. On the other hand, thin thicknesses may be critical for a good shielding effect, but, as seen from Equation (16), if the material has high magnetic permeability (μ) or high electric conductivity (σ), the skin depth is smaller, and as a result, it can reveal a significant contribution of SE_A . Moreover, as the radiation frequency increases, the conductor becomes increasingly perfect and impenetrable to electric fields.^[32]

2.1.3. Multiple Reflections

The multiple reflection mechanism is happening if the thickness of the shield is lower than the skin depth, most of the EMW is reflected at the first boundary. The EMW that passed through it can be reflected again at the second boundary, thus the multiple reflections (SE_M), as shown in Figure 2c, which are calculated as follows^[31]

$$SE_M = 20\log\left(1 - e^{-\frac{2t}{\delta}}\right) \quad (18)$$

It is seen that the SE_M depends on the ratio between thickness and skin depth, and is related to the SE_A . Hence, the contribution of SE_M is neglected if $\delta \ll t$ or if $SE_A \gg 10$ dB.^[31,33] However, in the presence of a magnetic field, as mentioned before, most of the incident EMW crosses the first boundary of the shield, and consequently, the SE_M should be considered in the calculation of total EMI SE.^[31]

2.2. Experimental Determination of the EMI Shielding Properties

When the EMW strikes a shielding, its energy is divided into reflected (R), absorbed (A), and transmitted (T) energy. These power coefficients are quantitative and give the real capability of the material to reflect, absorb, and transmit EM waves and follow the law of power balance

$$R + A + T = 1 \quad (19)$$

Experimentally, such coefficients are determined from a 2-port vector network analyzer by measuring scattering parameters (S) which describe the input–output relationships between ports in an electrical system. The input voltage and the forward voltage gain are defined by S_{11} and S_{21} , respectively, which then allows determining the R and T coefficients by means

$$R = |S_{11}|^2 \quad (20)$$

$$T = |S_{21}|^2 \quad (21)$$

From the R and T coefficients it is possible to determine the absorption coefficient (A)

$$A = 1 - R - T \quad (22)$$

Such coefficients allow for then the quantitative determination of the SE as follows

$$SE_R \text{ (dB)} = 10\log\left(\frac{1}{1-R}\right) \quad (23)$$

$$SE_A \text{ (dB)} = 10\log\left(\frac{1-R}{T}\right) \quad (24)$$

Given these values, it is possible to calculate the total EMI SE (SE_T) of the material^[1,9,34]

$$SE_T \text{ (dB)} = SE_R + SE_A \quad (25)$$

As mentioned before, if $\delta \ll t$ or $SE_A \gg 10$ dB, the contributions from SE_M are neglected.

When EMI shielding properties of a certain material are evaluated, it is crucial to distinguish the data given by Equations (19)–(22) and Equations (23)–(25). Among the thousands of pre-reviewed research on EMI shielding materials that can be found in the literature, it is quite common to use the values of SE_R or SE_A to classify the predominant EMI shielding mechanism. However, the power coefficients R or A are what give a comprehensive understanding of the EMI shielding performance because they are quantitative characteristics of the power balance, whereas SE_R , SE_A , and SE_T are relative quantities that represent the ability of the material to reflect, absorb or transmit EMW.^[35]

Finally, the EMI shielding efficiency can be calculated as^[9]

$$\text{Shielding efficiency(\%)} = 100 - \left(\frac{1}{10^{SE/10}}\right) \times 100 \quad (26)$$

but within mind the importance of the thickness and density of the shield, it is worth determining the specific SE (SEE) and absolute SE (SEE_t) that take the form^[9]

$$SEE \text{ (dB cm}^3\text{g}^{-1}\text{)} = \frac{\text{EMI SE}}{\text{density}} \quad (27)$$

$$SEE_t \text{ (dB cm}^2\text{g}^{-1}\text{)} = \frac{SEE}{t} \quad (28)$$

The EMI shielding properties of a certain material should be calculated for materials with an electrical conductivity of at least 1 S m^{-1} , the minimum required for practical applications of EMI shielding materials.^[1] In terms of classification as an EMI shielding material, typically, for commercial applications, 20–40 dB is the minimum effective range, a 40–60 dB range is considered a good EMI SE, and values above 60 dB are considered excellent.^[34,36]

2.3. Green EMI Shielding Effect

Based on the description of the different mechanisms that lead or not to the occurrence of the EMI shielding effect, undoubtedly electrical conductivity plays a crucial role in this phenomenon. However, a high electrical conductivity despite the result of a high EMI SE may limit the real-world application of the material. This is because the conductive materials cause greater and stronger reflection and consequently, EM pollution will certainly disturb the normal operation of other electronic devices and harm living organisms. As such, the need arises to explore the most effective strategy to produce materials that simultaneously have low reflection and allow for a high EMI shielding effect. In this sense, Cao et al. proposed the concept of the green shielding material which defines a material that shields EMW primarily by absorption, and this classification is based on the determination of the green g_s ^[28]

$$g_s = \frac{1}{S_{11}^2} - \frac{S_{21}^2}{S_{11}^2} - 1 \quad (29)$$

A material could be considered a green and efficient EMI shielding when $SE > 30$ dB and $SE_R < 3$ dB (or $R > 0.5$). In these

types of materials, the g_s also should be greater than 1 and up to 9. These characteristics cause that the most of incident EMWs to be absorbed by the shielding.^[28]

3. Processing Strategies for EMI Shielding MXene-Based Materials

3.1. Vacuum-Filtration Method

Vacuum-filtration is a simple processing technique that is commonly used in the production of high-purity MXene materials, as an EMI shielding reported for the first MXene ($Ti_3C_2T_x$) by Gogotsi and his team in 2016.^[9] This paves the way for research on MXenes for EMI shielding applications. In a research work, a 45 μm thick $Ti_3C_2T_x$ film fabricated by vacuum-filtration technique exhibited an outstanding EMI SE of 92 dB in the X-band frequency range (8–12 GHz). The EMI performance of the fabricated MXene was ascribed to i) an excellent electrical conductivity of MXene ($4600 S cm^{-1}$), which causes most of the EMWs to be reflected when strikes the surface of MXene, and ii) its laminate structure since the EMW passes through the surface of MXene layer and interacts with the high electron density of MXene, inducing eddy currents and ohmic losses. In addition, the surface termination groups also contribute to dipole polarization, thus increasing the attenuation of the EMW by absorption. In another work, a series of MXene films with thicknesses of ≈ 1 –15 μm were prepared to study the effect of elemental composition, layer structure, and transition-metal arrangement on their EMI shielding properties.^[10] A thickness of 10 μm different MXenes of M_2XT_x (Ti_2CT_x and V_2CT_x), $M_3X_2T_x$ ($Ti_3C_2T_x$, Ti_3CNT_x , and $Mo_2TiC_2T_x$), and $M_4X_3T_x$ ($Nb_4C_3T_x$ and $Mo_2Ti_2C_3T_x$) achieved an EMI SE higher than 20 dB, except Nb_2CT_x . Although the Ti-based MXenes exhibited higher SE_T values (i.e., 70 dB for $Ti_3C_2T_x$ with 14 μm thickness) probably because of their better-optimized synthesis process, it was found that a higher electrical conductivity and EMI shielding can be adjustable via changing the number of chemical composition or by increasing the number of layers in the MXene structure. For instance, despite the similar elemental composition of $Nb_4C_3T_x$ with Nb_2CT_x , it demonstrates a higher EMI SE at all film thicknesses in comparison to the other one. The same trend also was found for Ti_2CT_x and $Ti_3C_2T_x$. In this context, even though the $Ti_3C_2T_x$ MXene possesses the highest electrical conductivity, it did not provide the greatest value of EMI shielding. Alternatively, it already has been proven that the Ti_3CNT_x MXene provides an outstanding EMI SE of 116 dB which is the highest value reported for MXenes so far.^[37]

From the point of view of electrical conductivity changes of MXenes synthesized by the vacuum-filtration technique, it could be notified that the electrical conductivity of the as-synthesized material is sensitive and subject to an annealing treatment at different temperatures. For instance, it was observed that at 250 $^{\circ}C$ of annealing the conductivity of the Ti_3CNT_x MXene was increased from 1125 to 2475 $S cm^{-1}$. However, the opposite effect was observed when the heat treatment of annealing temperature was increased to 350 $^{\circ}C$, resulting in a reduced electrical conductivity of 1786 $S cm^{-1}$. On the one hand, gas expansion during thermal treatment could produce a porous structure with lower electrical conductivity. Such a porous structure provided several

interfaces for internal reflections for its application in EMI shielding. Thus, an efficient EMI shielding effect was observed in the porous structure of MXene together with an improvement in its oxidation resistance due to the removal of functional groups from the surface. The contribution of dipole polarization losses created by the remaining surface terminations and the formation of dielectric titanium dioxide (TiO_2) on the surface of Ti_3CNT_x were also considered to justify the enhanced absorption as described in previous research on the annealing treatment of MXenes.^[12]

Hybrid structures prepared by vacuum filtration have also been reported and their design is related to the issue of improving the mechanical properties of an MXene film, an important characteristic for real EMI shielding applications. Therefore, MXenes films have been reinforced by other fillers like graphene oxide (GO) or carbon nanotubes (CNT) to achieve a high-strength hybrid structure. In this regard, Liu et al. reported a $Ti_3C_2T_x$ -GO film with a high tensile strength of 209 MPa, while its electrical conductivity was maintained close to that of pristine MXene film ($3300 S cm^{-1}$). Thus, an EMI SE of 50.2 dB was achieved at a small film thickness of 7 μm .^[38] Such improvements can be attributed to the interfacial reinforcement of the MXene-GO hybrid film formed by abundant hydrogen bonds among the carboxyl, hydroxyl, and epoxide groups of GO and the polar groups ($-F$ and $-OH$) of MXene. The assembly of single-wall CNT (SWCNT) with $Ti_3C_2T_x$ in a ratio of 6:4 (CNT: MXene) led to an optimal EMI SE of 78.9 dB in a 55 μm thick composite, a result that can be attributed to the high aspect ratio and high electrical conductivity of CNT that form a continuous conductive network with MXenes.^[39] The good interfacial interaction between CNT and MXenes also allows for a significant improvement in mechanical properties compared to pure MXenes with an enhancement both in tensile strength and toughness with optimal values of 41.7 MPa and 0.89 $MJ m^{-3}$. These results show that the synergism between different fillers improves not only the mechanical properties of the composites but also the conductive network and multiple internal reflections result in an efficient attenuation of the EMW.

Although montmorillonite (MMT) has no electric conductivity, it is another good candidate for preparing MXene composites with excellent mechanical properties.^[40,41] Brick-and-mortar structures were produced either vacuum filtrating a mixture of $Ti_3C_2T_x$ /MMT^[40] or alternating layers of MMT-MXene-MMT in a sandwich film,^[41] and it was observed that the MXene nanosheets (NS) and MMT interact by hydrogen bond which facilitates the formation of a strong nacre-like structure. EMI shielding performances above 50 dB were obtained in the X-band, which may motivate future investigations of the use of environmentally friendly materials like MMT for meeting the EMI SE commercial requirements.^[34] Besides being an abundant and green material, MMT has the advantage of providing fire resistance properties, thus making it more advantageous over other fillers.

In addition to GO or CNT, the production of an MXene composite with good electrical and mechanical properties simultaneously can be made using ICP like poly(3,4-ethylene dioxythiophene) polystyrene sulfonate (PEDOT: PSS), polyaniline (PANI), or polypyrrole (Ppy). Liu et al. reported an ultrathin (11.1 μm) and flexible $Ti_3C_2T_x$ /PEDOT: PSS with an EMI SE of 42.1 dB and a tensile stress of up to 13.7 MPa.^[42] With a ratio of 7:1 (MXene: polymer), it is clear the enhancement of the mechanical

properties in this “brick-and-mortar” structure where the polymer act as a mortar and the MXene as a brick. Although MXene/polymer composite has a lower conductivity than pristine MXene, dipole polarization effects by PEDOT: PSS contributed to the attenuation of the EMW. With the same mass ratio of 7:1 but using PANI as a polymer matrix, a honeycomb structure in a $\text{Ti}_3\text{C}_2\text{T}_x/\text{PANI}$ composite favored the EMI shielding effect and mechanical properties as the composite with 40 μm in thickness reached an EMI SE of 36 dB and a tensile strength of 19.9 MPa.^[43]

Regarding the use of insulator polymer matrices, it is important to consider that the insulator polymer matrix may block the conductive properties of the MXene. Therefore, it is crucial to carefully control the dispersion of MXene within the polymer matrix. In addition, a poorly dispersed MXene may result in a mechanically weaker composite material overall.

Due to the large aspect ratio and high specific area of aramid nanofibers (ANF), strong interfacial adhesion with other materials, and stability in water that benefits self-assembly processes,^[44] it is of increasing interest in the production of MXene/ANF composites. In addition to the EMI shielding properties, it is relevant to mention that these brick-mortar structures, with MXene NS displaying the role of “brick” and ANF acting as “mortar,” can confer mechanical robustness and flexibility. Because of such mentioned facts, the MXene $\text{Ti}_3\text{C}_2\text{T}_x$ has been used to produce multilayered $\text{Ti}_3\text{C}_2\text{T}_x/\text{ANF}$ composites by vacuum-assisted filtration.^[45–48] The EMI SE performance of such composites ranged between 28 dB for a 17 μm thick composite^[45] and 79.8 dB with a thickness of 91 μm ^[47] in the X-band. In all these works, the influence of film thickness on EMI shielding properties was studied, and as expected, greater film thickness gives greater EMI shielding efficiency. However, for composites with 80 wt% of MXene, a 3.2 μm thick composite achieved an EMI SE of 40.6 dB,^[46] while a value of ≈ 28 dB was registered for a 17 μm in thickness produced by Xie et al.^[45] This difference may be due to the preparation of the suspension because according to the experimental description of both works, 2 weeks^[46] was the time defined to prepare the suspension that originated the composite with better performance versus 4 h^[45] for the thicker composite and with lower EMI SE value. Such difference is also noted in the mechanical properties with 66.3 and ≈ 100 MPa for 17 and 3 μm thick composites, respectively. Thus, a longer preparation time of the fiber suspension allowed for fibers with a higher aspect ratio and better dispersed to avoid their agglomeration. Upon mixing with the MXene suspension, it improved the synergism between the polymer matrix and filler, yielding a stronger interlayer hydrogen bonding and intra-layer interaction. Another strategy to improve the mechanical and EMI shielding properties can be from the alternating multilayered vacuum filtration of $n + 1$ parts ANF layer and n layers $\text{Ti}_3\text{C}_2\text{T}_x$.^[48] A composite with five layers of ANF and 4 of MXene, 20 μm of thickness, reached an EMI SE of 57.2 dB. At the same time, it is important to find a balance between the number of layers as a decrease to 53.0 dB was registered when one more layer of each material was added, and it is attributed to the prevalence of insulator properties of the ANF. Nevertheless, this kind of structure leads to more multiple reflections and interface polarization phenomena.

A double-layer structure of ANF- $\text{Ti}_3\text{C}_2\text{T}_x$ /silver nanowires (AgNW) was prepared via vacuum-assisted filtration followed by a hot-pressing approach.^[47] A suspension of $\text{Ti}_3\text{C}_2\text{T}_x/\text{AgNW}$ was

deposited on the top of the ANF layer, and then the double-layer structure was hot-pressed at 60 °C. The use of different MXene/AgNW contents allows to control of the thickness and therefore the EMI shielding properties as with an MXene/AgNW content of 20 wt%, the composite exhibited an EMI SE of 48.1 dB (45 μm) while a significant increase up to 79.8 dB (91 μm) was observed with the MXene/AgNW content of 80 wt%.

Alternatively to synthetic polymers, natural polymers like chitosan, natural rubber, and cellulose are other options when selecting a polymeric matrix that can confer excellent mechanical properties to the MXene-based composite. Besides being lightweight, biodegradable, nontoxic, and almost inexhaustible resources, their hydrophilicity, and abundance of functional groups are highly advantageous for strong interaction with MXenes by hydrogen bonding. Hence, it is evident its utilization in the production of polymer composites. Liu et al. fabricated an electrically conductive (14.02 S cm^{-1}) and EMI shield (34.7 dB) chitosan/ $\text{Ti}_3\text{C}_2\text{T}_x$ film at a thickness of 37 μm and using an MXene content of 75 wt% from a uniform solution by vacuum-filtration.^[49] With the same method but using natural rubber (NR), a composite can reach an EMI SE of 53.6 dB, with a similar electrical conductivity of 14.00 S cm^{-1} , but at a thickness of 251 μm .^[50] Even with the inclusion of CNT in a sandwich structure NR/MXene/CNT,^[51] the performance did not improve if compared to the last mentioned composite as it revealed an EMI SE of 49.9 dB and an electrical conductivity of 417 S cm^{-1} at a thickness of 200 μm . The agglomeration of CNT and MXene led to this lower performance, which is a recurring problem in the preparation of polymer composites.^[52,53]

As the use of cellulose, direct vacuum filtration of a homogeneous suspension of $\text{Ti}_3\text{C}_2\text{T}_x/\text{cellulose}$ nanofiber (CNF),^[54] alternating layers of CNF and MXene to obtain a multilayered^[55] or bilayered^[56] film has been used to produce MXene/CNF composites. Comparing the EMI shielding properties of these different composites, the bilayer structure performs better when the ratio of MXene/cellulose is 2:1 because the SE_T reached 60.1 dB at 12.4 GHz.^[56] However, such composite has a thickness of 100 μm , which is much higher compared to 47 μm MXene/CNF composite paper with an SE_T of 25.8 dB^[54] or multilayered film with a thickness of only 35 μm that exhibited an EMI SE of ≈ 40 dB.^[55] Thus, to improve the EMI shielding performance of thinner composites, the strategy may be to include another conductive filler in the composite, such as carbon nanotubes (CNT)^[57,58] or Ag particles.^[59–61] Either using an alternating layer strategy^[57,60] or a mixture solution^[59] to produce the MXene composite, it is clear that the introduction of another conductive filler enhances the connectivity between MXene NS by forming a continuous conductive network. In a research work by Cao et al., with the introduction of CNT, it was achieved an SE_T of 38.4 dB with a thickness of 38 μm ,^[57] while the presence of Ag nanoparticles (AgNP) led to EMI SE values of 50.7 (46 μm)^[59] and 55.9 (35 μm) dB.^[60] Dielectric losses by the terminal groups of MXenes, CNT or Ag particles, impedance matching between air present in the structure and filler interfaces, and more internal multiple reflections provided by the gradient structures are crucial for EMI shielding provided by vacuum-filtrated structures. The use of AgNP is also advantageous for providing antibacterial properties to the composite for EMI shielding applications in the field of wearable electronic devices to reduce the risk of bacteria

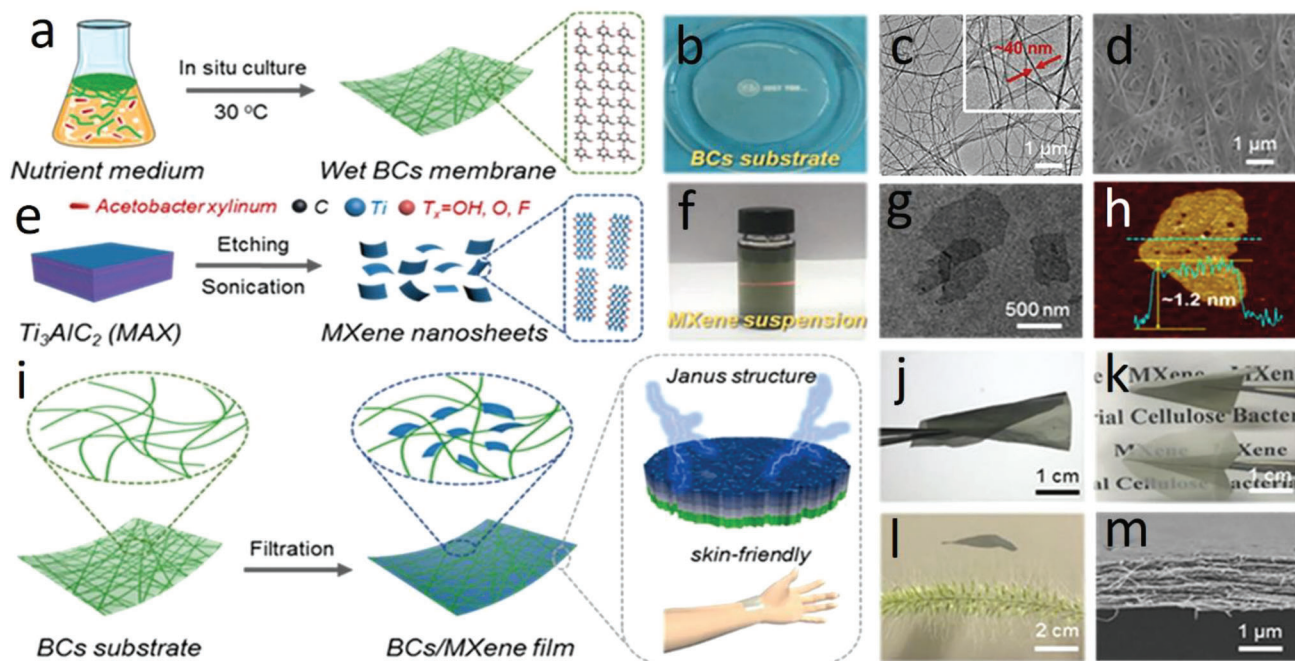


Figure 3. Fabrication of the BCs/MXene film. a) The wet BC membrane is prepared by in situ culturing acetobacter xylinum. b) Optical image of wet BC membrane. c) TEM image of BC. d) SEM image of BC substrate. e) $\text{Ti}_3\text{C}_2\text{T}_x$ MXene NS are fabricated from MAX (Ti_3AlC_2) phase using HCl and LiF. f) Optical image of MXene suspension. g) TEM and h) AFM images of $\text{Ti}_3\text{C}_2\text{T}_x$ MXene NS. i) Schematic of the BC/MXene film preparation process. j–l) Optical images show the flexible, ultrathin, and ultralight BCs/MXene films. m) The cross-section SEM image shows the lamellar structure of the composite film. Reproduced with permission.^[62] Copyright 2021, Elsevier.

transmission to human health.^[61] Thus, the same multilayered composite can show an excellent EMI SE of 61.9 dB with a thickness of only 30 μm and have excellent antibacterial properties.^[61]

Also, to produce wearable functional materials, bacterial cellulose (BC) has been used to produce skin-contactable materials.^[62,63] Ma et al. reported a thin Janus bacterial cellulose/MXene film (Figure 3) with only 1.7 μm by vacuum filtration with an SE_T of 20.2 dB and SEE_T of $\approx 69\,455.2 \text{ dB cm}^2 \text{ g}^{-1}$, which is one of the highest values reported for MXene-based transparent EMI shielding materials.^[62] Another work reported electronic skin based on a nanocellulose/ $\text{Ti}_3\text{C}_2\text{T}_x$ composite with good mechanical properties (124.6 MPa tensile strength), excellent biocompatibility, antibacterial properties, and an EMI SE of 36 dB.^[63] However, the thickness of that composite is 65 μm , which is much higher as compared to the ultrathin Janus structure reported by Ma et al., with a value of 1.7 μm .^[62] It seems that the vacuum filtration of an MXene suspension on a cellulose substrate several times is more advantageous for producing a thin electronic skin as compared to the vacuum filtration of a uniform suspension MXene/cellulose; nevertheless, future research should explore and compare these two approaches to better understand which one will be most advantageous for a scale-up process. With a low nanocellulose loading (0.167 wt%), a $\text{Ti}_3\text{C}_2\text{T}_x/\text{AgNW}$ composite film with only 16.9 μm thickness and a conductivity of $\approx 300 \text{ S cm}^{-1}$ reached an EMI SE of $\approx 42.7 \text{ dB}$,^[64] being another evidence that the use of green matrices and Ag particles may pave the way for MXene-based materials in wearable devices with antibacterial properties. Instead of cellulose, wood-pulp fabrics were directly decorated by $\text{Ti}_3\text{C}_2\text{T}_x$ NS through vacuum filtration together with the coating of hydrophobic methyltrimethoxysi-

lane (MTMS).^[65] This composite revealed an outstanding EMI shielding performance, with EMI SE values ranging from 57.8 to 90.2 dB, depending on the MXene content and fabric layers.

Research on annealing cellulose-based composites with $\text{Ti}_3\text{C}_2\text{T}_x$ NS obtained by filtration process has revealed that thermal treatment enhances the EMI shielding performance. Highly conductive hybrid films composed of multilayered $\text{Ti}_3\text{C}_2\text{T}_x$ MXene embedded with CNF/multiwalled CNT yarn-ball-shaped microspheres^[58] and intercalation of carbonized cellulose microspheres into $\text{Ti}_3\text{C}_2\text{T}_x$ MXene layers^[66] led to high efficient EMI shielding performance. The same research team also discovered that the vulcanization of $\text{Ti}_3\text{C}_2\text{T}_x$ MXene/natural rubber composite films could enhance their EMI shielding performance by up to 63.5 dB.^[67] In another work, the annealing treatment of hybrid films of intercalated buckminsterfullerene (C_{60}) into $\text{Ti}_3\text{C}_2\text{T}_x$ MXenes resulted in an EMI SE of 53.5 dB with a thickness of $18.7 \pm 0.55 \mu\text{m}$.^[68] It should be pointed out that the antioxidative properties of C_{60} enhanced the chemical durability of the hybrid films, which may extend the applications of MXenes-based hybrid materials with long-term durability. Overall, these results on thermal treatments could be useful for designing lightweight and high-performance EMI shielding materials.

All the above-mentioned works on MXene composites prepared by filtration techniques for EMI shielding applications have contributed significantly to the progress in this area. However, all these composites revealed a predominant reflection shielding mechanism which may limit real-world applications. For the absorption-predominant EMI shielding mechanism, it is based solely on the SE_A values, which is not always accurate without considering the determination of the power coefficients (R ,

A, and T). For instance, Iqbal et al. reported an enhanced absorption of EMW in $\text{Ti}_3\text{C}_2\text{T}_x$ films with segregated PS as a result of a uniform distribution of PS beads in the interlayer of $\text{Ti}_3\text{C}_2\text{T}_x$.^[69] It was determined that at the comparable thickness and same polymer content, the composite with a smaller PS bead size has a larger SE_A and SE_T values than those with larger bead sizes. However, without determining the power coefficients, it is inconclusive if such a composite does have a real EMW-absorbing capacity. This way, He et al. produced a flexible multilayered $\text{Ti}_3\text{C}_2\text{T}_x$ /hydroxyethyl cellulose ($\text{Ti}_3\text{C}_2\text{T}_x$ /HEC) film with an absorption-dominant EMI shielding mechanism (Figure 4a–c).^[70] The average values of R and A are 0.4 and 0.46, respectively (Figure 4d), being thus observed some advances in the production of green EMI shielding composites. In order to increase the absorption ability of an MXene-cellulose composite, the solution may lie in the introduction of a magnetic filler like FeCo in the composite because it can increase impedance matching, enrich magnetic losses and enhance the EMW absorption.^[71] A multilayered composite CNF- $\text{Ti}_3\text{C}_2\text{T}_x$ -FeCo with a conductive-magnetic gradient was produced (Figure 4e) and it showed a stronger ability to absorb EMW. Such an effect was enhanced by increasing the thickness of the magnetic layer, with the composite reaching an EMI SE of 58.0 dB (Figure 4f) and a R value of 0.61 (Figure 4g). Instead of using magnetic fillers to promote a greater absorption effect, Gong et al. fabricated a brick-mortar hierarchical structure where the presence of *n*-octadecane phase change capsules (PCC) allowed a decrease of the R values (Figure 4h).^[72] In this flexible film, the employed PCC acted as a brick, the $\text{Ti}_3\text{C}_2\text{T}_x$ as the sand, and the PVA as the cement.

The EMI shielding performance in the X-band of MXene film materials produced by the vacuum filtration-assisted method is summarized in Table 1.

3.2. Freeze-Drying and Foaming Methods

The synthesis of porous foam- and aerogel-based composites offers an opportunity to create materials with low density, large porosity, and high specific surface area, compared with films, which, combined with the high conductivity of MXenes, can achieve highly suitable EMI shielding materials. In this regard, Liu et al. produced the first flexible and lightweight $\text{Ti}_3\text{C}_2\text{T}_x$ MXene foam with a parallel, compact, and layered structure that achieved an impressive EMI performance of 70 dB when treated with hydrazine and heated at 90 °C.^[11] Furthermore, these MXene foams had a hydrophobic surface wettability, making them ideal for use in wearable electronics in wet environments. Although this method allows the production of materials with a wide range of pore sizes and a high surface area, the use of hydrazine can be potentially hazardous, and the process may require special handling and safety measures. Therefore, the freeze-casting method can be a suitable alternative for obtaining lightweight and porous MXene composites for EMI shielding applications.

An MXene aerogel with a density inferior to 10 mg cm⁻³ was fabricated via a freeze-casting route, showing an excellent EMI shielding performance of up to 75 dB and a specific SE of 9 904 dB cm³ g⁻¹, surpassing other foam-like materials reported in the literature.^[73] In that research work, the researchers also

mentioned that the material has a low reflection with a $\text{SE}_R < 1$ dB which is expected due to multiple reflections and scattering within the porous structure. However, as mentioned before, without the determination of the power coefficients, it is not possible to learn the real EMI shielding mechanism.

In another work, a bidirectional freeze-casting method was also used to produce different flexible and anisotropic MXene aerogels with long-range order of aligned lamellar structures.^[74] The $\text{Ti}_3\text{C}_2\text{T}_x$ aerogel had the highest EMI SE at 70.5 dB, followed by the Ti_2CT_x at 69.2 dB and the Ti_3CNT_x at 54.1 dB. The extremely low density of 0.0055 g cm⁻³ of the $\text{Ti}_3\text{C}_2\text{T}_x$ aerogel resulted in a high SSE_t of 88 182 dB cm² g⁻¹.

In the production of MXene-aerogel composites, electrical conductive $\text{Ti}_3\text{C}_2\text{T}_x$ porous architectures were created via GO-assisted hydrothermal assembly followed by directional freezing and freeze-drying at a low $\text{Ti}_3\text{C}_2\text{T}_x$ content of 0.74 vol%.^[75] A high electrical conductivity of 6.959 S cm⁻¹ and EMI SE values of over 50 dB were registered in the X-band.

Although MXenes are a perfect EMI shield against EMW because of their hydrophilic and electrically conductive properties, the weak interaction among MXene NS makes them difficult to form compressible 3D architectures with high conductivity. Hence, researchers have reported the use of polymer matrices, such as nanocellulose,^[76,77] polydimethylsiloxane (PDMS),^[78,79] polyurethane (PU),^[80] polyimide (PI),^[81] or reinforced fillers like CNT^[82,83] to overcome this limitation.

Zeng et al. created a nanocellulose/MXene biomimetic aerogel via a unidirectional freezing method.^[76] This process combined CNF with MXene NS to form a strong, hybrid aerogel. The hybrid aerogel formed featured oriented cell walls in the longitudinal plane and an isotropic structure in the transverse plane. Such architecture also contributed to enhancing conductivity between $\text{Ti}_3\text{C}_2\text{T}_x$ and CNF, which created a highly efficient EMI shield with an EMI SE of up to 74.6 dB. In fact, CNF could reduce the gaps between MXene resulting in the complete use of MXenes' conductivity and EMI shielding properties. Thus, CNF is superior in creating lightweight yet robust MXene-based aerogels without significant compromising effects on conductivity and EMI SE. In a recent research work by Wu et al.,^[77] it has been demonstrated that MXene-based aerogels reach an EMI SE of 42–81 dB at a density of merely 10–45 mg cm⁻³. It is reported a PDMS-coated MXene/sodium alginate (SA) foam with an electric conductivity of 22.11 S cm⁻¹ and an EMI shielding efficiency of 70.5 dB.^[78] The use of PDMS conferred structural stability to the composite as in a composite with 6.1 wt% of MXene it registered an EMI SE of 48.2 dB after 500 compression-release cycles. The combination of divalent metal ion-induced crosslinking, vacuum-assisted-filtration-induced self-assembly, and freeze-drying resulted in an aerogel composed of $\text{Ti}_3\text{C}_2\text{T}_x$ and calcium alginate with decent flexibility.^[84] At a thickness of 26 μm and 90 wt% of $\text{Ti}_3\text{C}_2\text{T}_x$, the composite exhibited an EMI SE of 54.3 dB and a SSE_t of 17 586 dB cm² g⁻¹. The structural stability of MXenes can be enhanced by an interfacial reinforcement approach as noticed by Liu et al.^[81] MXene/PI aerogel could provide outstanding mechanical flexibility and electrical conductivity. The $\text{Ti}_3\text{C}_2\text{T}_x$ NS were closely encapsulated by PI layers, forming a sandwich-structured framework through the efficient interfacial reinforcement of PI macromolecular chains. This outcome contributed to the formation of a ro-

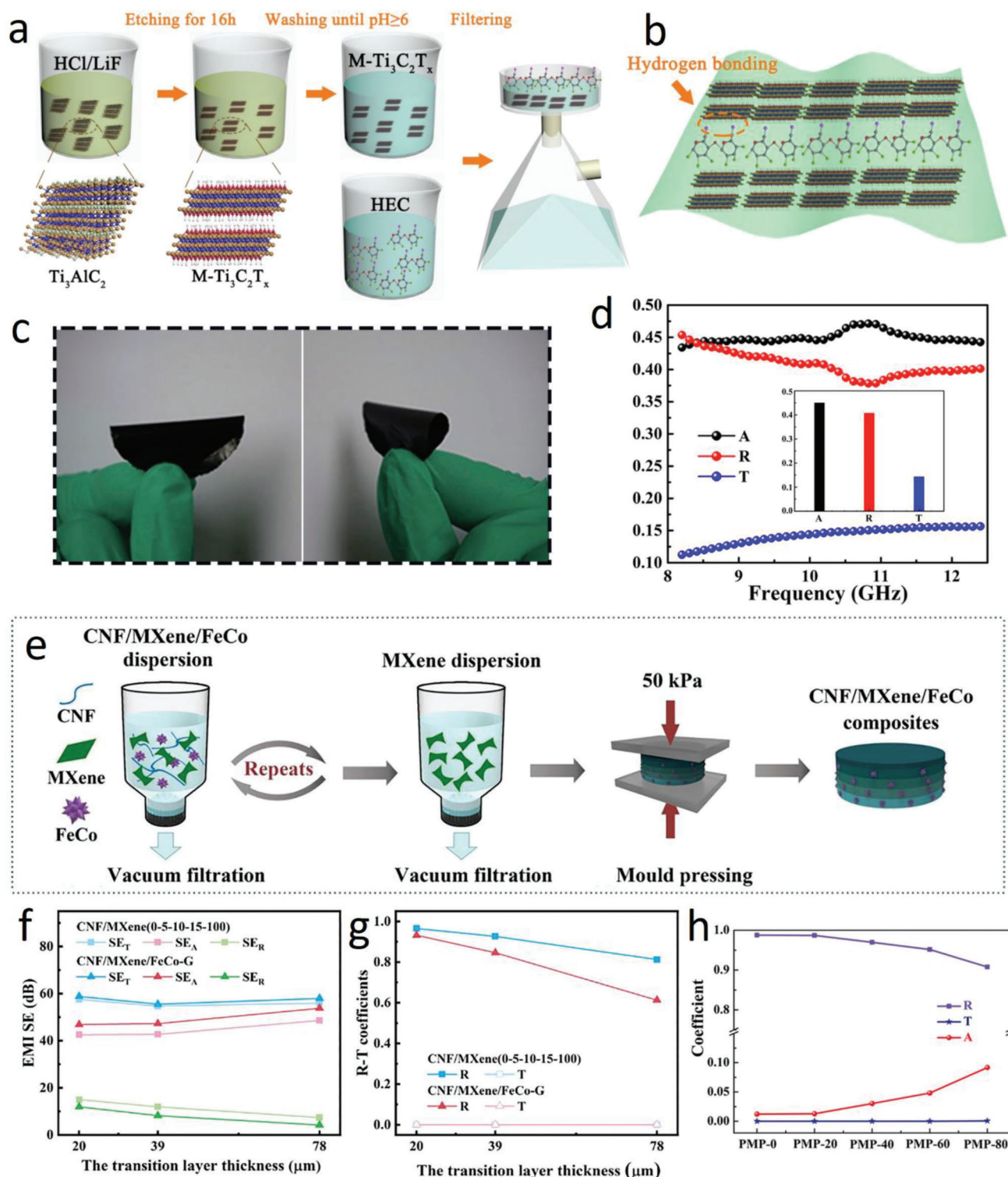


Figure 4. a) Schematic illustration of fabricating M-Ti₃C₂T_x/HEC composite film. b) Schematic of M-Ti₃C₂T_x/HEC composite film. c) Digital image of M-Ti₃C₂T_x/HEC composite film. d) The *A*, *R*, and *T* of M-Ti₃C₂T_x/HEC composite film. The inset shows the average *A*, *R*, and *T* of M-Ti₃C₂T_x/HEC composite film. Reproduced with permission.^[70] Copyright 2020, Elsevier. e) Schematic of the fabrication of CNF/MXene/FeCo gradient composite films. f) *SE_T*, *SE_R*, *SE_A*, and g) *R* and *T* values of the composite films with different transition layer thicknesses. Reproduced with permission.^[71] Copyright 2023, Elsevier. h) The *A*, *R*, and *T* coefficients in PVA/MXene/PCC films with different PCC contents. Reproduced with permission.^[72] Copyright 2022, Wiley-VCH.

Table 1. EMI shielding properties in the X-band of MXene film materials produced by vacuum filtration method.

Composition ^{a)}	Structure design	Thickness [μm]	Conductivity [S cm ⁻¹]	EMI SE [dB]	SSE/t [dB cm ² g ⁻¹]	Refs.
Heat-treated Ti ₃ CNT _x	Porous	40	1786	116.2	—	[37]
Heat-treated Ti ₃ C ₂ T _x		40	—	93.0	—	
Ti ₃ C ₂ T _x /NR		251	14.0	53.6	—	[50]
Ti ₃ C ₂ T _x	Layered	45	4600	92	—	[9]
Ti ₃ C ₂ T _x /SWCNT		56	1855	78.9	15 236.1	[39]
Ti ₃ C ₂ T _x		14	14 000	70	—	[10]
Ti ₃ C ₂ T _x /NR		54	—	63.5	—	[67]
Ti ₃ C ₂ T _x /cellulose		12.1	1672	59.8	18 637.1	[66]
Ti ₃ C ₂ T _x /CNF/MWCNT		25.1	392.6	51.8	12 011.8	[58]
Ti ₃ C ₂ T _x /C ₆₀		18.7	977.25	53.5	14 953.2	[68]
Ti ₃ C ₂ T _x /GO		7	2639	50.2	—	[38]
Ti ₃ C ₂ T _x /ANF		3.2	879	40.6	50 491.0	[46]
V ₂ CT _x		5	1000	≈40	—	[10]
Ti ₃ C ₂ T _x /Chitosan		37	14.02	34.7	—	[49]
Ti ₃ C ₂ T _x -AgNW/ANF	Bilayered	91	3726	79.8	5 379.9	[47]
Ti ₃ C ₂ T _x /CNF		100	59.4	60.1	—	[56]
Ti ₃ C ₂ T _x -AgNW/ANF		45	922	48.1	8 907.4	[47]
Ti ₃ C ₂ T _x /MMT	“Brick-and-mortar”	25	—	67	10 156.3	[40]
Ti ₃ C ₂ T _x /ANF		20	—	57.2	36 641.9	[48]
Ti ₃ C ₂ T _x /cellulose/AgNP		46	5.88	50.7	—	[59]
Ti ₃ C ₂ T _x /PVA		48	50	43.1	—	[72]
Ti ₃ C ₂ T _x /AgNW		17	≈300	42.7	16 724	[64]
Ti ₃ C ₂ T _x /PEDOT:PSS		11.1	340.5	42.1	—	[42]
Ti ₃ C ₂ T _x /nanocellulose		65	—	36	—	[63]
Ti ₃ C ₂ T _x /PANI		40	24.4	36	—	[43]
Ti ₃ C ₂ T _x /ANF		17	≈100	28	—	[45]
Ti ₃ C ₂ T _x /CNF		47	7.394	24	2 647.0	[54]
Ti ₃ C ₂ T _x /cellulose/AgNW	Sandwich	30	—	61.9	—	[61]
Ti ₃ C ₂ T _x /cellulose/AgNW		35	373.8	55.9	10 647.6	[60]
Ti ₃ C ₂ T _x /MMT		38.4	0.13	50	—	[41]
Ti ₃ C ₂ T _x /NR/CNT		200	4.17	49.9	1 885.5	[51]
Ti ₃ C ₂ T _x /CNF		35	≈0.82	39.6	7 029.0	[55]
Ti ₃ C ₂ T _x /cellulose/CNT		38	25.1	38.4	8 020.0	[57]
Ti ₃ C ₂ T _x /PS	Segregated	≈40	2 730	74	—	[69]
Ti ₃ C ₂ T _x /CNF/FeCo	Gradient	340	—	58	—	[71]
Ti ₃ C ₂ T _x /wood-pulp/MTMS	Decorated fabric	≈500	≈17.9	57.8	—	[65]
Ti ₃ C ₂ T _x /cellulose	Janus	1.73	5.1	20.2	69 455.2	[62]

^{a)} SWCNT—single wall carbon nanotubes; CNF—cellulose nanofiber; NR—natural rubber; MWCNT—multiwall carbon nanotubes; C₆₀—buckminsterfullerene; GO—graphene oxide; ANF—aramid nanofiber; AgNW—silver nanowires; MMT—montmorillonite; AgNP—silver nanoparticles; PVA—poly(vinyl alcohol); PEDOT: PSS—poly(3,4-ethylene dioxthiophene) polystyrene sulfonate; CNT—carbon nanotubes; PS—polystyrene; MTMS—methyltrimethoxysilane; PANI—polyaniline.

bust network, and more importantly, promising EMW absorption properties. Fabrication of 8.2 wt% Ti₃C₂T_x/AgNWs/epoxy aerogel led to an enhanced loss in EMI because of i) good compressible properties, ii) polarization loss induced by local defects, and iii) dipole and interface polarization caused by the accumulation of disparate charges between MXene and AgNWs.^[85] MXene/AgNWs aerogels can effectively reduce the magnitude of the incident EMW (EMI SE of 79.3 dB) and convert the radiation into thermal energy when they are connected to a porous conductive network (15.32 S cm⁻¹) in epoxy. An analogous performance for

all selected fillers was observed in a Ti₃C₂T_x/nickel ferrite/PU aerogel which registered an EMI SE of 64.7 dB and SSE_d up to 15 620 dB cm² g⁻¹.^[80]

As for the use of CNT, it was fabricated porous Ti₃C₂T_x/CNT aerogel via a bidirectional freezing method yielding excellent electrical conductivity of 9.43 S cm⁻¹ and an excellent EMI SE value of 103.9 dB at 3 mm thickness at the X-band frequency—the best value reported for synthetic porous nanomaterials.^[82] Furthermore, the exceptional improvement of the compressional modulus by 9661% compared with that of the pristine MXene

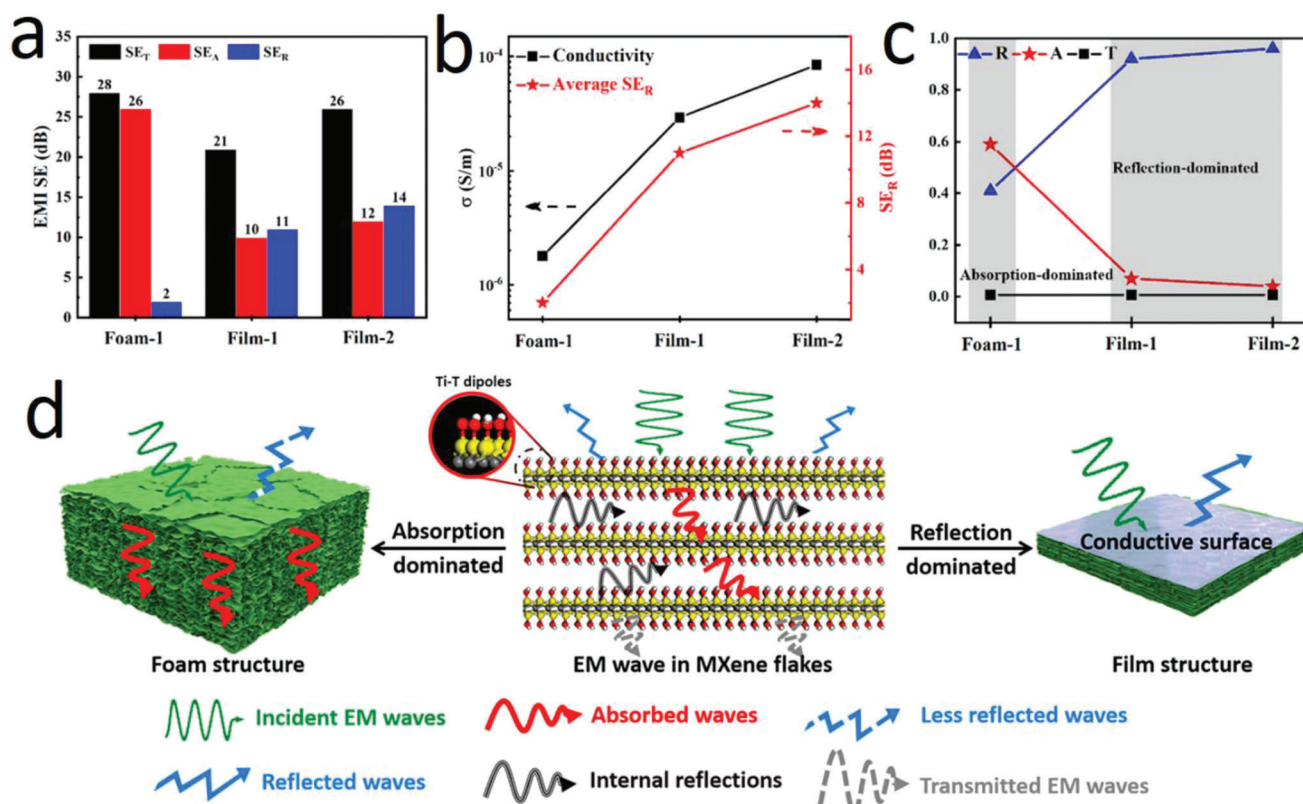


Figure 5. a) EMI SE_T , SE_A , and SE_R for Ti_2CT_x/PVA composites. b) Average SE_R and conductivity of $f-Ti_2CT_x/PVA$ composites. c) The proportion of R , A , and T coefficients in $f-Ti_2CT_x/PVA$ composites. d) Proposed EMI shielding mechanism of MXene/PVA composites with foam or film structure. Reproduced with permission.^[88] Copyright 2019, American Chemical Society.

aerogel was attributed to the uniform porous cellular framework supported by vertical pillars, which ensures deformation of the cell walls on compression rather than sliding between the walls. Such enhancement of the structural stability MXene/CNT aerogels was also observed by Deng et al.^[83] It was another evidence that the synergetic effect between MXenes and CNT not only benefits the mechanical properties but also contributes significantly to the achievement of a conductive network. It was discovered that only with 0.3 vol% filler content a 2 mm thick composite reached a conductivity of 4.472 S cm^{-1} and an EMI shielding efficiency of $\approx 51 \text{ dB}$. The increase of the filler amount up to 0.59 vol% led to an excellent SE_T of 90 dB.

When producing such porous structures, it is important to consider the effect of water on the shielding effect. This was investigated in hydrogel-based EMI shieldings composed of $Ti_3C_2T_x/PVA$.^[86,87] It was realized that the abundant water-enriched pores can increase the multiple reflections of incident EMW and enhance the polarization loss capability derived from water molecular and hydrogen-bond networks. Moreover, with plentiful water incorporated into the porous hydrogels, the EMI SE greatly outperformed the corresponding cellular foams/aerogels with the same building framework. In this context, a SE of $\approx 0.4 \text{ dB}$ was registered for a freeze-dried PVA aerogel, while the EMI SE of pure PVA hydrogel was $\approx 17 \text{ dB}$,^[87] making hydrogels more advantageous for producing EMI shielding. An outstanding performance of 91 dB was registered for the

$Ti_3C_2T_x/PVA$ hydrogel at a thickness of 7.5 mm in the broadband of 8.2–40 GHz.

Although these efforts in the development of conductive cellular structures with excellent EMI SE values in which the porous architecture favors the attenuation of EMW through multiple reflection and dipole polarization events, the high conductivity of the composites led to the reflection of most of the EMW. Such an effect is not desired because it generates EMI pollution, and thus it remains a challenge to produce absorption-dominated EMI shielding MXene-porous composites. So far Yin et al. have fabricated an MXene/PVA foam via freeze-drying of MXene/PVA hydrosol, and the foam with a thickness of 5 mm possessed EMI SE in the range of 26–33 dB with a filler content of only 0.15 vol%.^[88] The value of SE_R was determined to be $\approx 2 \text{ dB}$ and the R coefficient of about ≈ 0.4 . Although the reflection increased with the compression of the foam (Figure 5a–c), such work provides good insight into the preparation of lightweight MXene composites as EMI shields. It is suggested an absorption-dominated EMI shielding mechanism (Figure 5d) in which the porous structure of aerogels enables an improved impedance match leading to reduced EMW reflection. The EMW entering the interior of the foam experiences internal reflection due to its porous structure as well as the layered MXene NS, promoting EMW dissipation. Multiple internal reflections enhance the dissipation of the EMW through dipolar and interfacial polarization, therefore, a powerful absorption performance.

Table 2. EMI shielding properties in the X-band of porous MXene materials produced by foaming and freezing methods.

Composition ^{a)}	Method	Thickness [μm]	Conductivity [S cm ⁻¹]	EMI SE [dB]	SSE/t [dB cm ² g ⁻¹]	Refs.
Ti ₃ C ₂ T _x	Foaming method	60	580	70	53 030	[11]
Ti ₃ C ₂ T _x /CNT	Freezing method	3000	—	103.9	—	[82]
Ti ₃ C ₂ T _x /PVA		8500	—	94.2	—	[86]
		7500	—	91	—	[87]
Ti ₃ C ₂ T _x /CNF		2000	—	81.4	9 039	[77]
Ti ₃ C ₂ T _x /AgNW/epoxy		3000	15.32	79.3	—	[85]
Ti ₃ C ₂ T _x		—	22	75	—	[73]
Ti ₃ C ₂ T _x /CNF		2000	—	74.6	46 600	[76]
Ti ₃ C ₂ T _x		1000	—	70.5	64 182	[74]
PDMS-coated Ti ₃ C ₂ T _x /SA		2000	22.11	70.5	—	[78]
Ti ₃ C ₂ T _x /nickel ferrite/PU		2000	—	64.7	—	[80]
Ti ₃ C ₂ T _x /rGO		2000	6.959	56.4	—	[75]
Ti ₃ C ₂ T _x /calcium alginate		26	338.32	54.3	17 586	[84]
Ti ₃ C ₂ T _x /CNT		2000	4.472	51	—	[83]
Ti ₃ C ₂ T _x /PVA		5000	8.3 × 10 ⁻⁸	28	5 136	[88]

^{a)} CNT—carbon nanotubes; AgNW—silver nanowires; CNF—cellulose nanofiber; PDMS—polydimethylsiloxane; SA—sodium alginate; PU—polyurethane; rGO—reduced graphene oxide; CNT—carbon nanotubes; PVA—poly(vinyl alcohol).

The EMI shielding performance in the X-band of MXene porous materials produced by foaming and freeze-drying methods is summarized in Table 2.

3.3. Printing of MXenes

As presented, aerogels and foams can provide the desired EMW absorption effect, in addition to their low weight and good mechanical strength. However, their production is restricted to the use of specific forming molds or templates, which may limit, for example, electrical conductivity and polarization effects as it does not allow for adjustment of the size and location of the pores, the thickness of the structure or even the total area of the printed structure. To overcome the issue, printing techniques have emerged as a facile route for additive manufacturing which includes extrusion printing strategies such as inkjet printing, screen printing, direct ink writing (DIW), and 3D printing to name a few.^[89]

Inkjet printing has advantages such as compatibility with a wide range of substrates, including flexible and soft surfaces, low operating temperatures, and the capacity to print large area patterns with different shapes. Controlled material deposition, rapid multimaterial processing, and high-resolution digital patterning capability are other benefits of using such a technique.^[89,90] Vural et al. employed inkjet printing to print Ti₃C₂T_x inks as stimuli-responsive electrodes onto different substrates (cellulose paper, glass, polyethylene terephthalate (PET), and poly(methyl methacrylate) (PMMA)).^[91] MXene electrodes printed on PET substrates revealed electrical conductivity values as high as 1 080 S cm⁻¹, which is maintained after extreme bending deformation, and reached EMI SE values of up to 50 dB at film thicknesses of 1.35 μm, as a result of their excellent electrical conductivity and layered structure.

In screen printing, materials are deposited by squeezing high-viscosity inks through a stencil screen onto substrates, and it is

crucial for manufacturing integrated multifunctional devices by synthesizing functional inks without the use of expensive and complicated equipment.^[89] By adjusting the weight ratio between exfoliated Ti₃C₂T_x and xanthan gum, aqueous MXene inks have been created by Wu et al.^[92] These eco-friendly hybrid inks provided variable viscosity, great printability, and long-term stability. The hybrid inks showed high conductivity (480 S cm⁻¹), and great mechanical flexibility, and can be screen-printed into a variety of designs. This allows for the creation of multifunctional devices with an EMI SE of 40.1 dB that is maintained after 1000 cycles of bending at a thickness of 12 μm. A promising result was published regarding the surface functionalization of MXene with properly pre-polymerized polydopamine (PDA). Inspired by mussel adhesive proteins and nature melanin, PDA was used to protect MXene from water and oxygen, enrich surface chemistry, and enhance intersheet interactions. In addition, ideal rheological properties present an inspiring way for EMW modulation beyond just efficient EMI shielding as it reached 30 dB overall in the X-band at a thickness of around 14 μm (6 printing times) and conductivity of 161 S cm⁻¹.^[93]

The DIW also requires the use of MXene ink but it enables the preparation of a 3D structure with customized configurations. The solidification of the extruding ink can occur by freeze-drying and/or supercritical drying.^[94] Wu et al. produced robust and conductive MXene 3D frames with printable Ti₃C₂T_x/AIOOH inks.^[95] The printed frameworks were freeze-dried after the removal of electrically insulating AIOOH nanoparticles by immersion in AlCl₃/HCl solution, and the resulting robust and porous MXene frameworks exhibited tuned EMI SE in the range of 25–80 dB by adjusting printing parameters. For instance, by changing the filament spacing from 1.5 to 1.0 mm, the EMI SE increased from 62.7 to 71.5 dB. A further reduction in spacing to 0.5 mm resulted in a SE_T of 80 dB at a thickness of 1.37 mm in the whole X-band, and electrical conductivity of 53.2 S cm⁻¹. Dai et al. prepared an MXene/GO ink that delivered a 3D architecture with an electrical conductivity of 10.13 S cm⁻¹ and a broadband

tunable shielding efficiency of above 60 dB in the frequency range of 8.2–26.5 GHz by controlling the number of printing layers.^[96] Furthermore, the porous composite also exhibited outstanding reversible compressibility of up to 90% strain as well as excellent cyclic fatigue resistance, beneficial properties to protect electronic circuits from extra impact. To enhance the printability of MXene inks, SA was used to develop an aqueous MXene/SA ink and print aerogel meshes with customized geometries at a low MXene concentration.^[97] Cross-linking with calcium ions enhanced the mechanical and conductive properties of the printed aerogel meshes. The resultant aerogel mesh provided outstanding structural stability in water, and its compressive fracture strength is higher than that of pristine MXene aerogel mesh. The printed structures exhibited excellent conductivity with a value of 28.5 S cm⁻¹ being registered for an aerogel with 4 layers. With increasing the layer numbers of the printed aerogel mesh, an ultra-high EMI SE of 100.9 dB was achieved at a thickness of 2010 μm, which means that more than 99.99 999 999% of the incident EMW can be shielded. This fabricated composite supplies one of the best EMI shielding performances among similar structures. Another way to directly 3D print ultralight architectures with low-concentration of MXene can be by preparing an emulsion-based ink. The aqueous dispersion of Ti₃C₂T_x NS was added into the oil phase dissolved octadecyl amine (ODA), leading to electrostatic interactions between ligands and MXene NS.^[98] This leads to the formation of nanoparticle surfactants that assemble at the oil-water interfaces that have sufficiently high binding energy to afford to jam the 2D material and form stable emulsion droplets with enhanced rheological properties. This enabled the direct 3D printing of the emulsions into macroscopic architectures with an electric conductivity of 4.03 S cm⁻¹ and EMI shielding of 64 dB at a low concentration of 4.1 mg cm⁻³ and thickness of 2700 μm.

Despite these significant contributions, issues associated with material consumption, manufacturing time, and process scale-up can limit their application in EMI shielding applications. Therefore, computer-programmed software designing combined with printing technology may be a solution to fabricate advanced composites with desired structures and properties. In light of these, fused deposition modeling (FDM) is widely used in 3D printing including in the preparation of MXene composites with EMI shielding properties. Precise, mold-free, and low-cost fabrication of complex objects through layer-by-layer material deposition are advantages of 3D printing.^[99] In a Ti₃C₂T_x/MnFe₂O₄/multiwalled CNT-reinforced thermoplastic PU (TPU) composites, the MXene and MnFe₂O₄ hybrid fillers were built initially by an electrostatic bonding strategy, followed by adding MWCNT.^[100] The absorption of MnFe₂O₄ onto MXene NS can not only enhance the magnetic loss of the composite and improve the impedance matching of the material but also reduce the strong van der Waals forces between MXene NS. The high aspect ratio and excellent electrical and mechanical properties of MWCNT enable the construction of a 3D conductive network, thus acting as a bridging agent with MnFe₂O₄-coated MXene within the polymer matrix. The authors investigated the effects of porosity on the EMI SE value at a thickness of 2.1 mm and noticed that the EMI SE performance decreased with increased porosity, mainly because increasing porosity has led to the weight reduction of the composite material. The average EMI SE of the composites with 0%, 25%, 50%, and 75% porosity were 31.2, 29.1,

28.4, and 25.8 dB, respectively. With these results, it is seen that the FDM allows controlling key parameters like cell density and pore diameter which influence the EMI shielding performance of porous materials. The optimization of such parameters combined with thickness control by FDM could be an alternative for future research in the development of lightweight MXene composites with higher absorption, because, as already mentioned, porous structures provide more internal multireflections and, consequently, higher absorption of EMW. Furthermore, printing holds particular promise for high-rate and low-cost manufacturing of EMI shielding materials.

3D printing of hydrogels is also possible in an FDM printer in the fabrication of a hydrogel based on Ti₃C₂T_x-functionalized PEDOT: PSS, as reported by Nicolosi and coworkers.^[101] Inks with excellent printability were simply achieved at a low solid concentration of PEDOT: PSS and MXene, 4 and 1 wt%, respectively. The printed objects were then directly transformed into conductive and robust hydrogels with high shape fidelity by a freeze-thawing method. With that frozen and thawed treatment in the H₂SO₄ solution, the Ti₃C₂T_x-functionalized PEDOT: PSS revealed flexibility, stretchability, fatigue resistance, and high design freedom and shape fidelity (Figure 6a,b). The SEM images (Figure 6c–e) confirmed that the microscopic structures of the printed devices had not been significantly affected by the post-treatment, with only a minor volume change observed depending on the H₂SO₄ concentration. The conductivity of the hydrogel increased with the H₂SO₄ concentration, which brought to a high conductivity of 55.2 S cm⁻¹ and an EMI SE of 51.7 dB (Figure 6f,g) at a thickness of ≈295 μm. All of these findings show that the porous structure of the hydrogel combined with its water-rich environment contributed to a greater attenuation of the EMW (Figure 6h). The same benefits caused by the presence of water in a hydrogel, i.e., polarization loss by hydrogen bonds, combined with the porous structure also contributed to the shielding effect in a Ti₃C₂T_x/poly(acrylic acid)/calcium carbonate (Ti₃C₂T_x/PAA/ACC) hydrogel that served as ink for printing.^[102] The presence of ACC contributed to hydrogen bonding with the MXene and the chelation between PAA chains, resulting in a cross-linked structure. An absorption-dominated EMI shielding mechanism was confirmed in the terahertz band (0.2–2.0 THz), another proof that water generates polarization losses in both the giga- and terahertz bands, which can extend the use of MXene-based hydrogels in terahertz technologies.

Table 3 summarizes the EMI shielding performance of MXene composites produced by printing methods.

3.4. Electrospinning

The production of a flexible film with a high surface area, controlled thickness, mechanical strength, excellent flexibility, and light weight is particularly important for wearable and portable electronic EMI shielding materials, in which good flexibility is needed to ensure high mechanic deformations. The electrospinning technique can provide these properties by producing electrospun nanofibrous membranes.^[103–105]

The concept of electrospinning was proposed by William Gilbert in 1600, based on the formation of a cone-shaped water droplet in the presence of an electric field.^[104] Only from

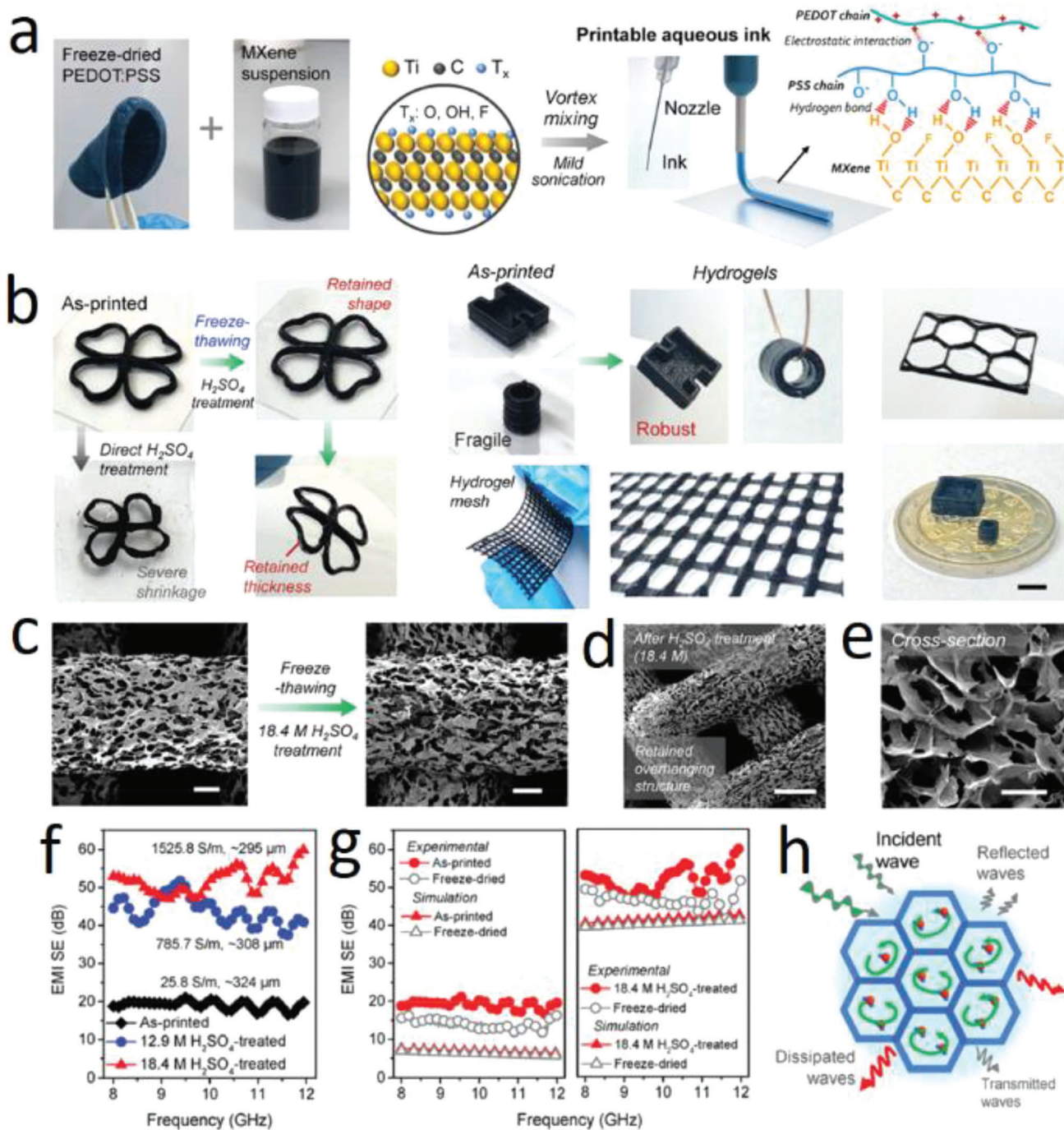


Figure 6. a) Scheme illustrating the preparation of MXene-functionalized PEDOT: PSS ink for extrusion printing. b) Photographs of the as-printed architectures before and after different post-treatments. c) SEM images of the printed filament before and after the freeze-thawing and 18.4 M H_2SO_4 treatments. d,e) SEM images of the printed hydrogel samples, showing that the microstructure is well-retained after freeze-thawing and 18.4 M H_2SO_4 treatment. f) EMI SE performance in the X-band). g) Simulated and experimental EMI SE of hydrogel and corresponding foam sample. h) Scheme of shielding mechanism. Reproduced with permission.^[101] Copyright 2021, Wiley-VCH.

the 1900s, greater advances have been achieved, with patents describing a prototype of the setup for electrospinning by John Cooley^[106] and William Morton,^[107] followed by a few years later with the patents by Anton Formhals^[108,109] disclosing the improvement in equipment, moving toward the commercialization

of electrospinning for the fabrication of textile yarns, or finally with the pioneering work by Geoffrey Taylor between 1964 and 1969 describing the formation of Taylor cone.^[110–112] This technology is relatively versatile and easy to operate, allowing the production of continuous and long fibers with diameters ranging

Table 3. EMI shielding properties in the X-band of MXene materials produced by different printing methods.

Composition	Method	Thickness [μm]	Conductivity [S cm^{-1}]	EMI SE [dB]	SSE/ t [$\text{dB cm}^2 \text{g}^{-1}$]	Refs.
$\text{Ti}_3\text{C}_2\text{T}_x$ /PET substrate	Inkjet printing	1.35	1080	50	—	[91]
$\text{Ti}_3\text{C}_2\text{T}_x$ /SA	DIW	2010	28.5 ^{a)}	100.9	4 709.1	[97]
$\text{Ti}_3\text{C}_2\text{T}_x$ /AlOOH		1370	53.2	80	—	[95]
$\text{Ti}_3\text{C}_2\text{T}_x$ /rGO scaffold		2700	10.1	79.3 ^{b)}	5 758.9	[96]
$\text{Ti}_3\text{C}_2\text{T}_x$ /ODA		2700	4.03	64	57 494	[98]
$\text{Ti}_3\text{C}_2\text{T}_x$ /Xantham gum	Screen printing	12	480	40.1	—	[92]
$\text{Ti}_3\text{C}_2\text{T}_x$ /PDA		≈ 14	161	30	—	[93]
$\text{Ti}_3\text{C}_2\text{T}_x$ -functionalized PEDOT:PSS	FDM	≈ 295	55.2	51.7	—	[101]
$\text{Ti}_3\text{C}_2\text{T}_x$ -MnFe ₂ O ₄ /MWCNT@TPU		2100	—	25.8	—	[100]

^{a)} Value for an aerogel with a thickness of 697 μm ; ^{b)} In the frequency range of 8.2–26.5 GHz; PET—polyethylene terephthalate; SA—sodium alginate; rGO—reduced graphene oxide; ODA—octadecyl amine; PDA—polydopamine; PEDOT: PSS—poly(3,4-ethylene dioxathiophene) polystyrene sulfonate; MWCNT—multiwall carbon nanotubes; TPU—thermoplastic polyurethane.

from micrometers to nanometers, implemented in many industrial companies nowadays.

The basic setup for electrospinning requires a high-voltage power supply (either direct current or alternating current), a syringe pump, a spinneret (metallic needle), and a grounded collector (conductor metallic drum). When a high voltage is applied, up to 30 kV, the polymer solution is forced out of the needle which will be highly electrified. As the voltage increases, the solution droplet begins to elongate into a conical form known as a “Taylor cone,” and it is ejected from the tip toward the metallic collector. During its trajectory, the fluid jet is subjected to radial repulsive charges that cause it to split into small filaments, a process called splaying. Depending on the solution viscosity, the jet solidifies with solvent evaporation and solid fibers will form, resulting in a nonwoven fiber mat covering the collector.^[103–105]

3.4.1. Electrospun Fibers for EMI Shielding Materials

The formation and diameter control of electrospun fibers is influenced not only by the processing conditions, such as the applied voltage, the flow rate of the solution, and the distance between the tip of the spinneret and the collector, but also by the properties of the selected materials used during the process (solvent, polymer matrix, and filler). The ambient conditions, humidity, and temperature also affect the process. Hence, it is important to understand the role of all these parameters in the EMI shielding properties of MXene-based materials.

With the use of a polymer matrix, a high aspect ratio, specific surface area, and molecular orientation will provide better mechanical properties to the electrospun fibers. These morphological properties, combined with the high porosity and low density, result in abundant interfacial sites which are beneficial for enhancing the EMI shielding effect by absorption, thus an adequate green shielding index. It is also expected an enhancement of the SEE_r due to the low density and low thickness of the MXene-based composites, important parameters in the production of lightweight EMI shielding materials.

The polymeric matrices typically used in electrospinning are insulating such as polyacrylonitrile (PAN), poly(vinyl alcohol) (PVA), and cellulose; however, it is usually required an additional

carbonization process for producing carbon nanofibers (CNF). These carbon fibers are electrically conductive because the high-temperature treatment used, usually between 600 and 1300 °C, restores the sp^2 carbon network. Yet, this reduction is not sufficient to form a conductive network that allows an effective EMI shielding effect. As such, the need arises to use electrically conductive fillers like MXenes. Poly(vinylidene fluoride) (PVDF) has also been used in the production of electrospun fibers, particularly the β -phase PVDF,^[113] being a good choice for producing EMI shielding materials due to its large intrinsic polarization and dielectric properties. Superior hydrophobicity, anticorrosion resistance, and excellent flexibility are other properties of this polymer matrix that expand its application real world.^[114]

The dispersion of MXenes within polymer matrices like PVA and cellulose leads to the formation of hydrogen bonds with terminal groups of $\text{Ti}_3\text{C}_2\text{T}_x$, thus, improving the mechanical properties of the composite. On the other hand, these insulator matrices decrease the electrically conductive properties of the composite as compared to a pure MXene film. Therefore, it may be necessary to carry out post-treatments of the electrospun MXene-fibers and/or combine other methods such as the embedded method, dip-coating deposition, vacuum filtration deposition, and spray deposition.^[115,116]

3.4.2. Electrospun MXene-Based Composites

Embedded Method: In the embedded method, MXene NS are uniformly dispersed in the spinning polymer solution, and then electrospun to produce an MXene-polymer composite. Besides improving the dispersion of the filler in the polymer matrix, it also reduces the oxidation rate of MXene, yielding highly oriented fibers, thus improving the mechanical properties of the composite.

Based on the fact that sandwich-structured EMI shielding materials can concentrate electric or magnetic fillers in one or more layers and contribute to a more effective EMI shielding mechanism. Zhang et al. fabricated sandwich-structured nanocomposite films using electrospinning-laying hot pressing technology, where Fe_3O_4 /PVA composite electrospun nanofibers were applied in the top and bottom layers and $\text{Ti}_3\text{C}_2\text{T}_x$ /PVA composite

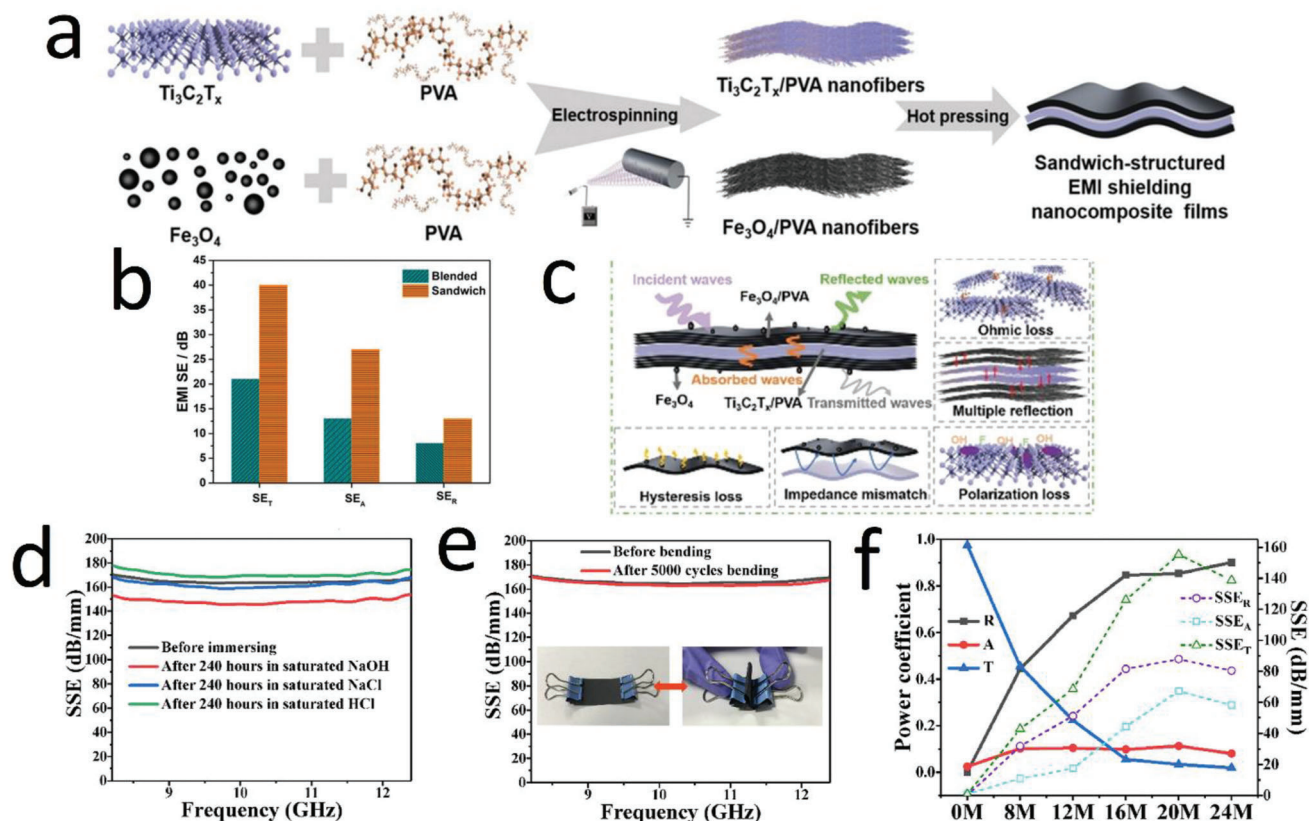


Figure 7. a) Schematic diagram of the preparation process for sandwich-structured $\text{Fe}_3\text{O}_4/\text{Ti}_3\text{C}_2\text{T}_x/\text{PVA}$ films. b) Comparison of EMI SE of blended and sandwich $\text{Fe}_3\text{O}_4/\text{Ti}_3\text{C}_2\text{T}_x/\text{PVA}$ films. c) Schematic diagram of EMI shielding mechanism of sandwich-structured EMI shielding nanocomposite films. Reproduced with permission.^[117] Copyright 2021, Wiley-VCH. d) EMI SEE of MXene/PVDF-HFP composite with 20 wt% MXene before and after immersion into saturated NaOH, NaCl, and HCl for 10 days. e) Flexibility and cyclic bending stability test of MXene/PVDF-HFP composite with 20 wt% MXene. f) Power coefficients and SEE_R , SEE_A , and SEE_T components of MXene/PVDF-HFP composites with different wt% of MXene from their average values in X-band. Reproduced with permission.^[118] Copyright 2022, Elsevier.

electrospun nanofibers in the interlayer (Figure 7a).^[117] Due to the electrospinning process and sandwich structure, when the amounts of $\text{Ti}_3\text{C}_2\text{T}_x$ and Fe_3O_4 were only 13.3% and 26.7%, respectively, the EMI SE of the sandwich structure reached 40.0 at 12.4 dB with a thickness of 75 μm . This value of EMI SE was higher than that of the blended composite ($\text{Fe}_3\text{O}_4/\text{Ti}_3\text{C}_2\text{T}_x$)/PVA (21 dB) prepared with the same amount of fillers (Figure 7b). The electrospinning process arranged Fe_3O_4 and $\text{Ti}_3\text{C}_2\text{T}_x$ along the radial direction of the PVA electrospun nanofibers, which enhances the likelihood of the formation of magnetic, electrical, and thermal conduction paths. When EMW is incident on the top magnetic layers, they will interact with magnetic Fe_3O_4 in the $\text{Fe}_3\text{O}_4/\text{PVA}$ electrospun nanofibers, resulting in hysteresis loss. After passing through that layer, the large impedance mismatch between the $\text{Fe}_3\text{O}_4/\text{PVA}$ and $\text{Ti}_3\text{C}_2\text{T}_x/\text{PVA}$ layers originates a reflection back of the EMW with a new hysteresis loss occurring. The remaining EMW will face ohmic loss and polarization loss (because of the functional groups presenting in the MXene) as they go through the $\text{Ti}_3\text{C}_2\text{T}_x/\text{PVA}$ layer due to the multiple electrospun nanofibers. This EMI shielding mechanism is illustrated in Figure 7c. The researchers claimed that these repeated reflections and scattering greatly enhance the EMW absorption ability of the sandwich-structured EMI shielding nanocomposite film

by determining a higher SE_A (Figure 7b). However, the determination of the power coefficients R and A is missing, which renders the actual EMI shielding mechanism inconclusive. Nevertheless, the sandwich-structured nanocomposite films had exceptional thermal conductivities and mechanical characteristics, which increases the prospect of producing sandwich structures by electrospinning for EMI shielding applications.

By varying the $\text{Ti}_3\text{C}_2\text{T}_x$ concentration between 8 and 24 wt% in poly(vinylidene fluoride-co-hexafluoropropylene) (PVDF-HFP), Liu et al. produced EMI shielding fabrics with an absolute SE (SEE_d) of 160 dB mm^{-1} in the X-band which remains unchanged when exposed to different media (acidic, alkaline, and saline).^[118] Considering the application of the composite as a wearable material, it was tested in the above-mentioned media for 10 days to simulate the contact of different fluids with the human body, rainwater, or sweat. It was found that the saline solution (NaCl) did not change the performance of the EMI shielding, while the NaOH solution slightly deteriorated probably due to possible oxidation of the MXene (Figure 7d). On the other hand, the SEE value improved with exposure to an acidic solution, which can be due to the proton exchange that benefited the electrical conductivity. It is also important to highlight the protection conferred by the polymer matrix to achieve such results. The EMI shield-

ing performance was also evaluated after repeated bending and noticeable variance were not observed (Figure 7e). Although the researchers state that the material is environmentally robust, the R coefficient is much higher than A for all the composites (Figure 7f), which does not favor a green shielding index.

Dip-Coating Deposition: Dip coating is a simple process that involves immersing the electrospun fibers in a solution with the desired material to be impregnated, in this case, MXene, for fabricating multifunctional layers. The high surface area and porosity of the fibers significantly improve the impregnation of the MXene NS.

Among the published works on EMI shielding MXene materials using dip-coating, Wang et al. have reported the use of polydopamine (PDA) in the modification of electrospun fibers which were then impregnated with an MXene solution.^[119–121] PDA improves surface adhesion because of the numerous surface functional groups ($-\text{OH}$ and $-\text{NH}_2$), thus the chemical activity on substrates,^[119] which in these studies, enhances the absorption of MXene solution. Production of the $\text{Ti}_3\text{C}_2\text{T}_x$ -coated composites consists of electrospinning of PAN fibers with dispersed Ni^{120} or TiO_2 ,^[119,121] followed by their modification with PDA, immersion in the MXene solution, and finally in the PDMS solution. The final impregnation of PDMS makes the sandwich structure hydrophobic and confers stability to it. The EMI SE values for these composites range from 28.8^[121] to 37.7^[120] dB. This improvement of EMI shielding performance in the sandwich structure composed of Ni particles,^[120] seems to be due to the deposition of an extra layer of polypyrrole (PPy) after modification of the PAN fibers with PDA. The PPy is an intrinsic conductive polymer and combined with the MXene layer resulted in an extra shielding interface, thereby more efficient against the effects of the EMW.

Using different loading contents of Fe_3O_4 and $\text{Ti}_3\text{C}_2\text{T}_x$, a solution of $\text{Ti}_3\text{C}_2\text{T}_x$ was dip-coated on an electrospun thermoplastic PU/PAN/ Fe_3O_4 composite.^[122] A maximum EMI SE of 32.5 dB was achieved by a composite with 20 wt% of Fe_3O_4 and 5 mg of MXene and a thickness of 450 μm , which allows concluding a major effect of the Fe_3O_4 in the EMI shielding effect since, for the same amount of MXene and lower Fe_3O_4 content, the EMI SE values are lower. This increase in EMI shielding efficiency also follows a higher R coefficient, thus a predominant reflection mechanism.

Vacuum Filtration Deposition: Electrospinning combined with vacuum filtration allowed the production of a flexible delaminated $\text{Ti}_3\text{C}_2\text{T}_x$ -CNF composite in which the thickness of the $\text{Ti}_3\text{C}_2\text{T}_x$ coating was controlled by the volume of the solution during vacuum-assisted filtration.^[123] The thickness of the MXene layer ranged from 6 to 15 μm , and as expected, the composite with a thicker $\text{Ti}_3\text{C}_2\text{T}_x$ coating exhibited the best performance, with an EMI SE of 42.7 dB in the frequency range of 2–18 GHz. The composite also showed good mechanical properties with excellent stability after being bent for 500 cycles. However, as has been mentioned throughout this review, again, the EMI shielding mechanism was explored through the SE_R and SE_A values which does not allow us to learn about the real EMI shielding mechanism. The same is observed in the research works by Yang et al.,^[124] and Zhang et al.,^[125] combined electrospinning with vacuum filtration to produce MXene composites with competitive EMI shielding performance and, in addition, superior thermal properties, a factor that is becoming more relevant. However,

without knowing the real shielding mechanism by determining the R and A power coefficients, their application in the real world is compromised.

On the other hand, Du et al. produced a multilayered $\text{Ti}_3\text{C}_2\text{T}_x$ /PLA composite that revealed that R is above 0.9 for all samples in the X-band due to the impedance mismatch between free space and conductive MXene layer.^[126] The composite with 150 μm in thickness reached an EMI SE of 55.4 dB. The material has a distinctive Joule heating performance with a rapid temperature response from 31 to 52.8 $^\circ\text{C}$ within 25 s at a low trigger voltage of 1.5 V, which is encouraging for wearable and portable electronics. Despite this, there is still a need to increase the shielding effect by absorption to obtain a material with a favorable green index.

Spray-Coating Deposition: In the spray-coating method, a thin layer of MXene NS is deposited onto the surface of the electrospun fibers by a spraying gun. The porous network structure of the electrospun fibers enables an effective penetration of the MXene NS, which can have a great effect on the EMI shielding properties of the composites under deformation.

This method has been used for producing sandwich structures as impedance matching between different layers, multiple reflections within the internal interfaces of the film cause the dissipation of EMW, being thus a structure with a good prospect for EMI shielding applications. Yuan et al. produced a $\text{Ti}_3\text{C}_2\text{T}_x$ /PU composite fabric in a procedure where the MXene solution was uniformly spray-coated onto a PU fabric with a thickness of 200 μm with an effort to obtain a material with favorable EMI shielding performance at a stretching process under large deformation, highly desired in flexible electronic devices.^[127] The researchers compared the EMI shielding performance of composites spray-coated on one side and both sides, naturally obtaining better results with the sandwich structure (EMI SE \approx 21 dB) due to the presence of a larger conductive network and more internal reflections inside the fabric. In addition to meeting the minimum EMI SE values to be considered for commercial applications (20 dB), this work reported the first flexible EMI shielding MXene material with a sandwich structure that can sustain a stable EMI shielding performance at a stretching process within 30% tensile deformation. It was characterized that the stacked MXene NS was kept connected and maintained the conductive network structure during the stretching process. This characteristic was due to the presence of multiple conductive sites in such a compact and ordered microstructure. At the same deformation, a $\text{Ti}_3\text{C}_2\text{T}_x$ -PU composite exhibited an EMI SE of \approx 30 dB by spray-coating with only one of the electrospun fabric sides.^[128] The MXene NS were tightly and self-adaptively coated on the surface of the fiber, creating an efficient conductive network on the TPU matrix. It contributed to a better EMI shielding performance by creating more internal multiple reflections and polarization sites that increased the attenuation of the EMW. Thus, it is possible to obtain improvements in EMI shielding just by spray-coating one side of the fabric. The high R coefficients in the range of 0.8–1 for different MXene loadings show that the reflection predominates the EMI shielding mechanism. It can be a limitation for wearable shielding fabrics as proposed in the research work.

Concerning the combination of spray-coating and hot-pressing, Zhang et al. produced a sandwich structure by spraying $\text{Ti}_3\text{C}_2\text{T}_x$ NS onto an electrospun AgNW-PI fabric which was

Table 4. EMI shielding properties in the X-band of MXene materials with different structures produced by electrospinning.

Composition	Structure design	Thickness [μm]	Conductivity [S cm^{-1}]	EMI SE [dB]	SSE/ t [$\text{dB cm}^2 \text{g}^{-1}$]	Refs.
$\text{Ti}_3\text{C}_2\text{T}_x/\text{CNF}$	Sandwich	150	29.8	55.4	—	[126]
$\text{Ti}_3\text{C}_2\text{T}_x/\text{PVDF-AgNW}$		—	$1.0 \Omega \text{ sq}^{-1}$	45.4	—	[124]
$\text{Ti}_3\text{C}_2\text{T}_x/\text{AgNW-PI}$		97	—	40.7	—	[129]
$\text{Ti}_3\text{C}_2\text{T}_x\text{-Fe}_3\text{O}_4/\text{PVA}$		75	1.2	40	—	[117]
$\text{Ti}_3\text{C}_2\text{T}_x/\text{PAN-TiO}_2$		45	62.2	37.7	14 779.9	[120]
$\text{PAN-Ni}/\text{PPy}/\text{Ti}_3\text{C}_2\text{T}_x/\text{PDMS}$		28	92.7	32	4 085.9	[119]
$\text{PAN-Ni}/\text{Ti}_3\text{C}_2\text{T}_x/\text{PDMS}$		29	71.9	28.8	12 422.4	[121]
$\text{Ti}_3\text{C}_2\text{T}_x\text{-Fe}_3\text{O}_4/\text{PAN}$		200	0.115	≈ 21	—	[127]
$\text{Ti}_3\text{C}_2\text{T}_x/\text{TPU}/\text{PAN}/\text{Fe}_3\text{O}_4$	Janus	75	—	66	—	[125]
$\text{Ti}_3\text{C}_2\text{T}_x/\text{Fe}_3\text{O}_4\text{-PI}$	Layered	15	45	42.7 ^{a)}	—	[123]
$\text{Ti}_3\text{C}_2\text{T}_x/\text{PLA}$		450	—	32.5	—	[122]
$\text{Ti}_3\text{C}_2\text{T}_x/\text{TPU}$		33	35.4	43.8 ^{b)}	9 221.2	[130]
$\text{Ti}_3\text{C}_2\text{T}_x/\text{AgNW-PI}$		300	—	≈ 30	—	[128]

^{a)} In the frequency range of 2–18 GHz; ^{b)} In the frequency range of 8–26.5 GHz; CNF—cellulose nanofiber; PVDF—polyvinylidene fluoride; AgNW—silver nanowires; PVA—poly(vinyl alcohol); PAN—polyacrylonitrile; TPU—thermoplastic polyurethane; Ppy—polypyrrole; PDMS—polydimethylsiloxane; PI—polyimide; PLA—polylactic acid.

then hot-pressed together with another AgNW-PI fabric to make a composite with a thickness of 97 μm .^[129] Actually, there is double protection of the metal particles against oxidation: the electrospinning process protects the AgNWs because they are coated by the polymeric matrix, while the MXene layer is protected by the two electrospun AgNW-PI fabrics. With the increase in the MXene loading, the composite reached a maximum EMI SE of 40.7 dB in the X-band. The EMI shielding performance of the composites was also evaluated after different thermal treatments of 100 and 200 °C. It was observed that the EMI shielding performance of the composite films gradually decreased as treatment time increased, and after high-temperature treatment for 48 h, the EMI SE of both samples decreased to 30 dB at the same time. This was attributed to the destruction of the conductive network due to oxidative fracturing of the AgNWs at high temperatures. Although the electrospinning process protects the AgNP from oxidation, improvements are needed to avoid the deterioration of EMI shielding properties at high temperatures. These EMI shielding evaluations of the thermally treated composites are suitable in real applications of these types of composites in aerospace, automotive, and aircraft fields where thermal stability at high temperatures is required.

More recently Yang et al. reported a bifunctional PAN fiber fabric decorated with a suspension of $\text{Fe}_3\text{O}_4@\text{MXene}$.^[130] Dopamine was polymerized onto a PAN fiber fabric and then spray-coated with a hybrid suspension of $\text{Fe}_3\text{O}_4@\text{MXene}$, with different Fe_3O_4 loadings. This composite with a thickness of 33 μm exhibited good EMI shielding performance with an EMI SE of 43.83 dB at a frequency of 8–26.5 GHz, where X-, Ku-, and K-bands are included. The EM shielding effect is greatly improved by the synergistic effect of magnetic loss induced by Fe_3O_4 and ohmic loss from the conductive MXene. Again, the porous structure and impedance matching between all the different layers contributed to multiple EM wave reflections and absorption within. Moreover, as compared to other shielding architectures with similar or larger thicknesses, such composite structure $\text{Fe}_3\text{O}_4@\text{MXene}/\text{PAN}$ demonstrated outstanding SSE_t of 9

212.1 $\text{dB cm}^2 \text{g}^{-1}$, combining thus lightweight and EMI shielding effect in the same material.

Table 4 summarizes the EMI shielding performance in the X-band of MXene composites produced by electrospinning.

3.5. Self-Assembly Methods

Self-assembly methods can also be used to produce MXene materials with high EMI shielding efficiency. Layer-by-layer (LbL), electrostatic or interfacial assembly are some examples of self-assembly procedures that have been employed to produce MXene materials for EMI shielding applications.

3.5.1. LbL Assembly

With the LbL technique, a composite material is created by depositing alternating layers of oppositely charged polymers and conductive NP. Strategies such as spin-spray coating,^[131] spin-coating,^[132] dip-coating,^[133–137] and spray-coating,^[138,139] have been employed during the LbL assembly to produce MXene composites with EMI shielding capabilities.

Spin-Spray Coating: Semitransparent films were produced by alternating layers of $\text{Ti}_3\text{C}_2\text{T}_x$ -PVA and SWCNT- or MWCNT-PSS dispersions.^[131] These films were created by spinning and spraying the layers onto a rotating glass substrate. The thickness and uniformity of the films were controlled by adjusting the amount of dispersion, the rotational speed of the substrate, and the number of $\text{Ti}_3\text{C}_2\text{T}_x$ -CNT bilayers. Such a number of bilayers also influenced the transparency of the film as it decreased with the increasing of the layers. In terms of EMI shielding properties, the presence of two conductive fillers like MXene and CNT led to an electrical conductivity of 130 S cm^{-1} and an absolute SSE_t of 58 187 $\text{dB cm}^2 \text{g}^{-1}$ for a 300 bilayer film with a thickness of about 200 nm.

Spin-Coating: In another study, chitosan solution and $\text{Ti}_3\text{C}_2\text{T}_x$ suspension were assembled alternatively along the

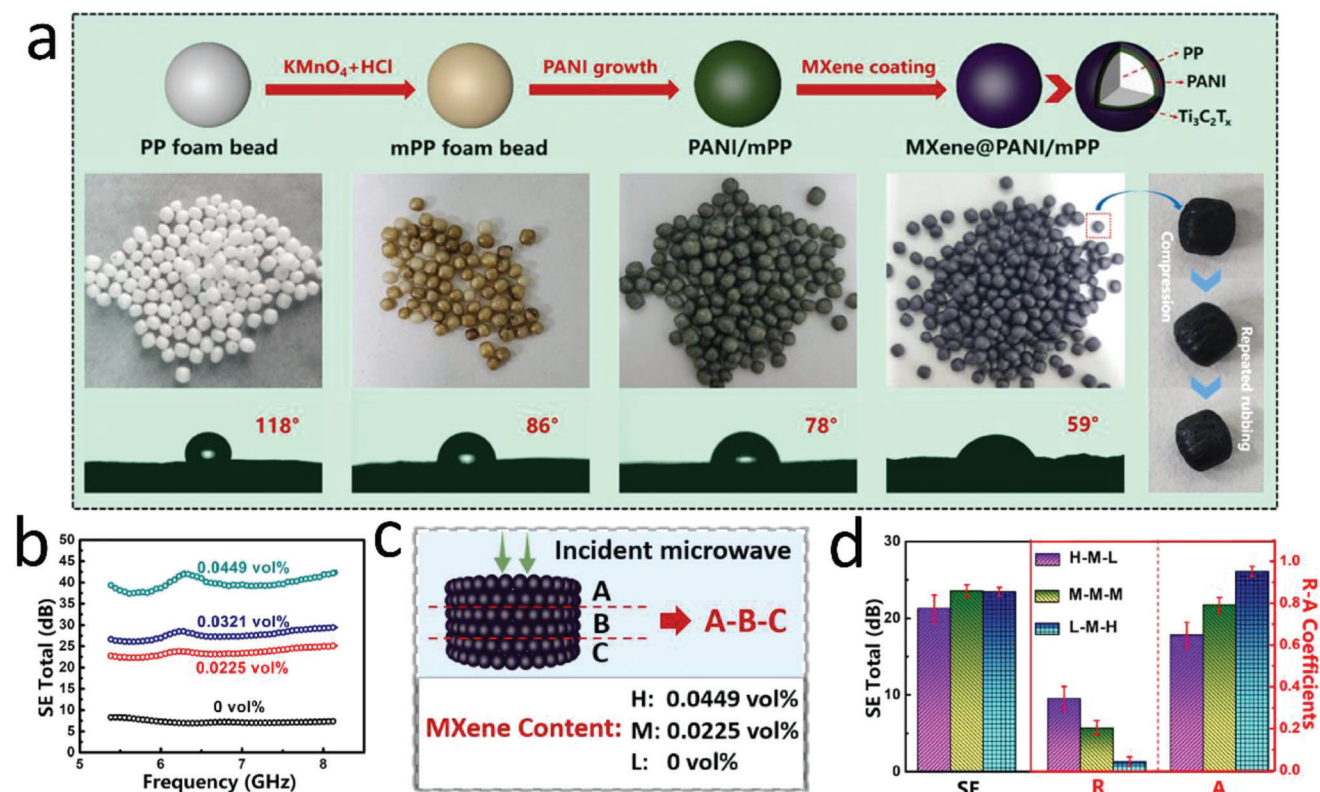


Figure 8. MXene@PANI/mPP foam beads: a) Schematic illustration of the fabrication process. b) EMI SE with different MXene loading at a thickness of ≈ 12 mm. c) Representation of the composite foams with asymmetric MXene networks. d) R-A coefficients of H-M-L, M-M-M, and L-M-H samples at a thickness of ≈ 12 mm. Reproduced with permission.^[79] Copyright 2021, Elsevier.

thickness direction by spin-coating,^[132] resulting in a 35 μm thick chitosan/MXene multilayer film with a maximum EMI SE of 40.8 dB and a high SSE_t of 10 650 $\text{dB cm}^2 \text{g}^{-1}$. For further investigation of EMI shielding performance, R and A coefficients were determined to be 0.52 and 0.42, respectively, indicating that most of the EMW are reflected. Nevertheless, the LbL method contributed to the absorption loss capacity of the composite. In addition to the electrically conductive and EMI shielding properties, the orderly stacked MXene NSs also contributed to superior thermal conductivity ($6.3 \text{ W m}^{-1} \text{ K}^{-1}$) and distinguished Joule heating performance, useful characteristics for some applications like aircraft deicing, wearable electrical heaters, and personal thermal management devices.

Dip-Coating: By using the dip-coating approach, it was observed that MXene-based conductive polymer composite (CPC) foams with high-efficiency EMI shielding performance and ultralow reflectivity could be attained.^[79] As shown in Figure 8a, compressible PP-based composite foams were fabricated by coating conductive MXene NS onto modified PP foam beads followed by the encapsulation of PDMS elastomer after orderly assembling the foam beads. The EMI SE values ranged from ≈ 23.5 to 39.8 dB (Figure 8b) with only ≈ 0.0225 – 0.0449 vol% MXene in the frequency range of 5.38–8.17 GHz including designated C-band. Initially, the power coefficient R was determined to be in the range of ≈ 0.20 – 0.31 , indicating an absorption mechanism. The construction of a gradient structure (Figure 8c) with different values of MXene loading demonstrated a R value of ≈ 0.05

with an almost unchanged EMI SE of ≈ 22.7 dB with an MXene content of ≈ 0.0225 vol. This value of MXene content is among the lowest values for effective EMI shields which have been ever reported. Such a result was obtained with an ascended-gradient configuration, contrasting with the high R coefficient of ≈ 0.31 in an ascended-gradient configuration as shown in Figure 8d. In another work, PI foams were immersed into $\text{Ti}_3\text{C}_2\text{T}_x$ dispersion followed by a chemical cross-linking approach agent of poly((phenyl isocyanate)-*co*-formaldehyde) (PMDI), allowing them to achieve a satisfactory EMI SE in the X-band.^[140] It was observed that with increasing density of the composite foams derived from excess MXene loadings, SE_T and SE_A were enhanced significantly and achieved 62.5 and 54.9 dB, respectively, at a density of 48.7 mg cm^{-3} and an SEE_t of $8567 \text{ dB cm}^2 \text{g}^{-1}$. Instead of a PI foam, a porous super aligned CNT skeleton was immersed in the $\text{Ti}_3\text{C}_2\text{T}_x$ dispersion, also followed by chemical-cross-linked of PMDI.^[141] Some improvements were observed in the production of low-density composites with a thickness of 6 μm . The composite structure exhibited an EMI SE of 49 dB and an SEE_t of $128 680 \text{ dB cm}^2 \text{g}^{-1}$. However, these works could not determine power coefficients to fully assess the shielding absorption contributions in the porous structures.

In the class of smart textiles, Wang et al. produced a hydrophobic and electrical conductive fabric that provides excellent EMI shielding by the in situ deposition of polymerized PPy-modified $\text{Ti}_3\text{C}_2\text{T}_x$ NS on a PET textile.^[135] A 1.3 mm thick PPy/MXene textile exhibited high electrical of 10 S cm^{-1} , allowing for an

exceptional EMI shielding efficiency of ≈ 90 dB due to the presence of MXenes as the PPy-coated PET textile only allowed for low electrical conductivity (0.03 S cm^{-1}). As a conductive material, PPy-coated PET textile is not efficient enough for EMI shielding applications, but when it is combined with the MXenes, PPy enhances the interfacial interactions between MXene NS and the PET fibers resulting the excellent EMI shielding performance.

Cotton fabrics have also been used to produce MXene-based composites by dip-coating,^[134,136,137] with SE values ranging from 20.1^[134] to 31.0 dB.^[136] As expected, increasing amounts of $\text{Ti}_3\text{C}_2\text{T}_x$ gradually achieved higher EMI shielding performance.^[136,137] However, simultaneously the composite retains the flexibility and air permeability characteristic of cotton demonstrating a good adhesion between MXene NS and substrate. Polyethylenimine (PEI),^[134,136] ammonium polyphosphate (APP),^[136] or phytic acid (PA) with high phosphate content^[137] are used as flame retardants, conferring good flame retardancy.

In another study, a carbon fiber fabric (CF) was treated with MXene dispersion and then immersed in an aniline solution to promote the in situ polymerization of PANI onto the MXene/CF surface.^[133] A 550 μm textile-based composite material presented an electrical conductivity of 0.2457 S cm^{-1} , EMI SE of 26.0 dB, and SSE of $135.5 \text{ dB cm}^3 \text{ g}^{-1}$.

From the results presented here on dip-coating, it can be said that it is a simple and scalable process. But at the same time, it is crucial to ensure good distribution and impregnation of the conductive MXene across the fabric surface. In this way, it will be possible to have better control over the total amount of MXene used, a factor that influences the total thickness of the conductive layer or layers. Although greater thickness provides a better shielding effect, it may adversely affect the flexibility of the composite which is crucial for smart textiles usually employed as wearables.

Spray-Coating: An important parameter to be considered in the coating of fabrics as potential EMI shields is the type of fabric used. Hence, Liu et al. fabricated an MXene-decorated silk-textile (M-silk) by alternately spray-coating of $\text{Ti}_3\text{C}_2\text{T}_x$ and AgNW onto both sides of a porous silk substrate (**Figure 9a**).^[138] A conductive ($0.8 \Omega \text{ sq}^{-1}$) and biomimetic leaf-like nanostructure—MXene NS and AgNW represent the lamina and vein, respectively (**Figure 9b**)—was created. **Figure 9c–e** shows the morphology of the obtained structure. It can be seen that an exceptional EMI shielding efficiency of ≈ 90 dB at 12.4 GHz with a thickness of 480 μm was achieved. Even at a thickness of 120 μm , the textile achieved an outstanding EMI SE value of 54 dB (**Figure 9f**). Considering that, in addition to the quality of the conductive network and thickness of the composite, the texture structure and tightness between the fiber bundles also influence the electrical and shielding properties.^[142] The effect of the substrate was also investigated by spraying the active fillers (MXene and AgNW) on cotton, nylon, and wool. Except for the cotton textile, all composites exhibited low sheet resistances of $\approx 2 \Omega \text{ sq}^{-1}$ and EMI shielding efficiencies between 38 and 46 dB (**Figure 9g**). Nevertheless, the silk fabric performs better because it shows an EMI SE higher than 40 dB at a smaller thickness ($\approx 120 \mu\text{m}$). Analyzing in detail the performance of the MXene/AgNW/silk composite, the presented good performance resulted from the synergistic effect between the MXene and AgNW as the MXene NS act as a conductive binder to closely connect the AgNW reducing

the contact resistance between the AgNW and thus providing a more stable and efficient conducting pathway. The use of MXene in the production of this composite has several advantages: i) weak interactions were noticed between AgNWs and the silk substrate in the absence of the 2D fillers, which deteriorates the conductive network, ii) it decreases the amount of AgNW, an expensive filler, thus decreasing the cost of the potential application in the real world, iii) MXene layer also protects the AgNWs from oxidation, giving the textile a sensitive humidity response, and creates self-derived hydrophobicity. The hydrophobic effect was further improved with a hydrophobic agent (1H,1H,2H,2H-perfluorooctyltriethoxysilane (POTS)), which did not affect the EMI shielding performance of the composite. Lightweight thin composite films made of cellulose provided also excellent shielding performance against EMI.^[139] The films were created using a process of spray-coating and chemical cross-linking, which involves uniformly spraying MXene aqueous dispersion on the surface of a cellulose film, followed by adding GO layers to improve the physical and chemical cross-linking. This results in strong hydrogen and Ti–O–C bonding interactions, which improve the mechanical strength, oxidation stability, and EMI SE. The thickness of the MXene layer was adjusted to achieve an EMI SE ranging from 20.6 to 71.0 dB in the X-band and exceeding 60 dB in the broadband frequency range of 8.2–40 GHz. These composite films also offer high SEE_t of $18\,837.5 \text{ dB cm}^2 \text{ g}^{-1}$, which is comparable to the best EMI shields reported.

3.5.2. Electrostatic and Interfacial Assembly

Concerning electrostatic self-assembly, $\text{Ti}_3\text{C}_2\text{T}_x$ /PS core-shell hybrids were produced by the electrostatic assembling of negative MXene NS on positive PS microspheres, followed by compression molding at 130 °C as illustrated in **Figure 10a**.^[143] **Figure 10b,c** shows that the electric conductivity and EMI SE improve with the increment of MXene content, registering an EMI SE value of 62 dB with 1.90 vol% of $\text{Ti}_3\text{C}_2\text{T}_x$ (**Figure 10c**). Such EMI shielding performance was achieved at 2 mm in thickness, while the 1 mm nanocomposite with the same MXene content registered only 27 dB. The strategy of producing core-shell structures was also followed by Vu et al.,^[144] with the electrostatic assembly of $\text{Ti}_3\text{C}_2\text{T}_x$ and rGO on PMMA beads surface and then hot-pressed at 180 °C. The well-ordered 3D network of MXene and rGO benefitted the conductive and EMI SE properties of the composites because, with a filler loading of only 0.5 vol%, the composite exhibited a conductivity of 1 S cm^{-1} and an average EMI SE of 27 dB, which is higher than the minimum requirement for some commercial applications. A filler content of 2 vol% exhibited EMI SE values higher than 51 dB over the whole X-band at a thickness of 2 mm. Additionally, the thermo-mechanical properties of the PMMA nanocomposites were improved by this 3D structure with a thermal conductivity in the range of 0.98–3.96 $\text{W m}^{-1} \text{ K}^{-1}$ and a storage modulus of 4.6 GPa.

Electrostatic self-assembly between MXene and GO NS was also performed by Tang et al.^[145] However, it was the thermal annealing at 800 °C that led to an electrical conductivity of $1\,958 \text{ cm}^{-1}$, EMI SE of ≈ 54.4 dB and an outstanding SSE_t of $27\,897 \text{ dB cm}^2 \text{ g}^{-1}$ at a thickness of only 15 μm .^[145] The rapid breakaway of polar functional groups on GO and $\text{Ti}_3\text{C}_2\text{T}_x$ induced the for-

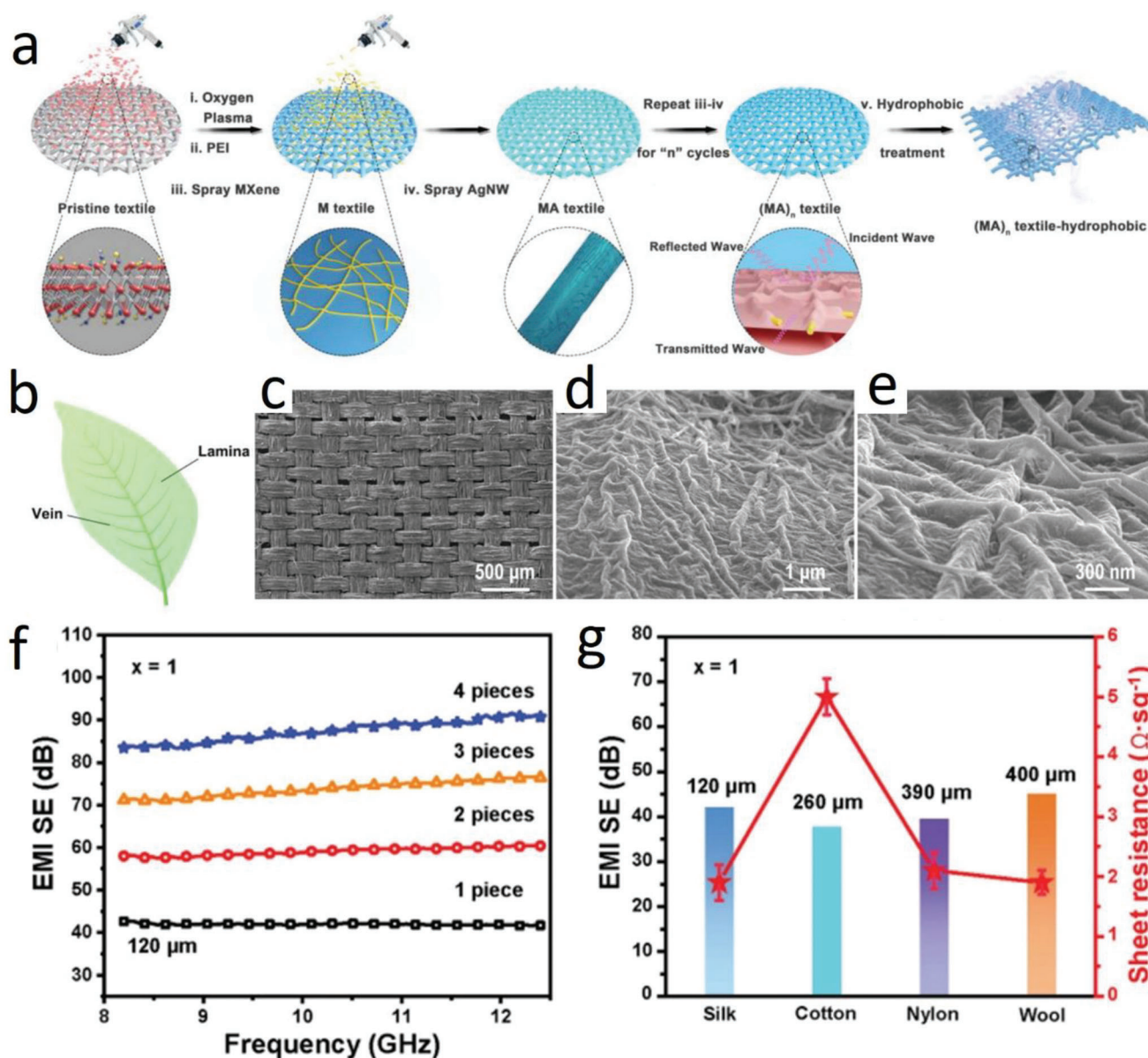


Figure 9. a) Schematic illustrating the fabrication of hydrophobic, permeable, and conductive silk textiles with a vacuum-assisted LbL assembly approach. In the designation $(MA_x)_n$ textile, x stands for the concentration of AgNW, n is the repeated numbers, and M and A represent MXene and AgNW, respectively. b) A leaf and c–e) SEM images of $(MA)_{20}$ silk under different magnifications showing the leaf-like network formed with MXene NS and AgNWs on silk substrate. f) EMI shielding performances of $(MA)_{10}$ silk textiles with different thicknesses. g) EMI shielding performances and sheet resistances of $(MA)_{10}$ textiles with different textile substrates (silk, cotton, nylon, and wool). Reproduced with permission.^[138] Copyright 2021, Wiley-VCH.

mation of a porous and conductive network, thus contributing to multiple interface reflections and polarization.

The same benefits of the thermal process were noticed in pristine MXene reported by Yun et al., who investigated the layer number-dependent EMI shielding behavior in nanometer-level thickness in $Ti_3C_2T_x$ -assembled films.^[146] As expected, increasing the number of layers improved the performance of its shield (Figure 10d), but it was with the 400 °C annealing that the improvements were most significant (Figure 10e). The researchers observed that a monolayer assembled film with an EMI SE of 1 dB

at 8.2 GHz, which corresponds to $\approx 20\%$ shielding efficiency, can be improved upon to 20 dB by using a 24-layer film of ≈ 55 nm thickness, meeting the commercial requirements of EMI shielding materials. Spin-coated MXene films were also prepared for comparison, revealing lower performance, in particular at thin thicknesses, which holds that the spin-coating process is more critical at lower thicknesses for producing a uniform film, therefore negatively influencing an efficient EMI shield.

Table 5 summarizes the EMI shielding performance in the X-band of MXene composites produced by different LbL methods.

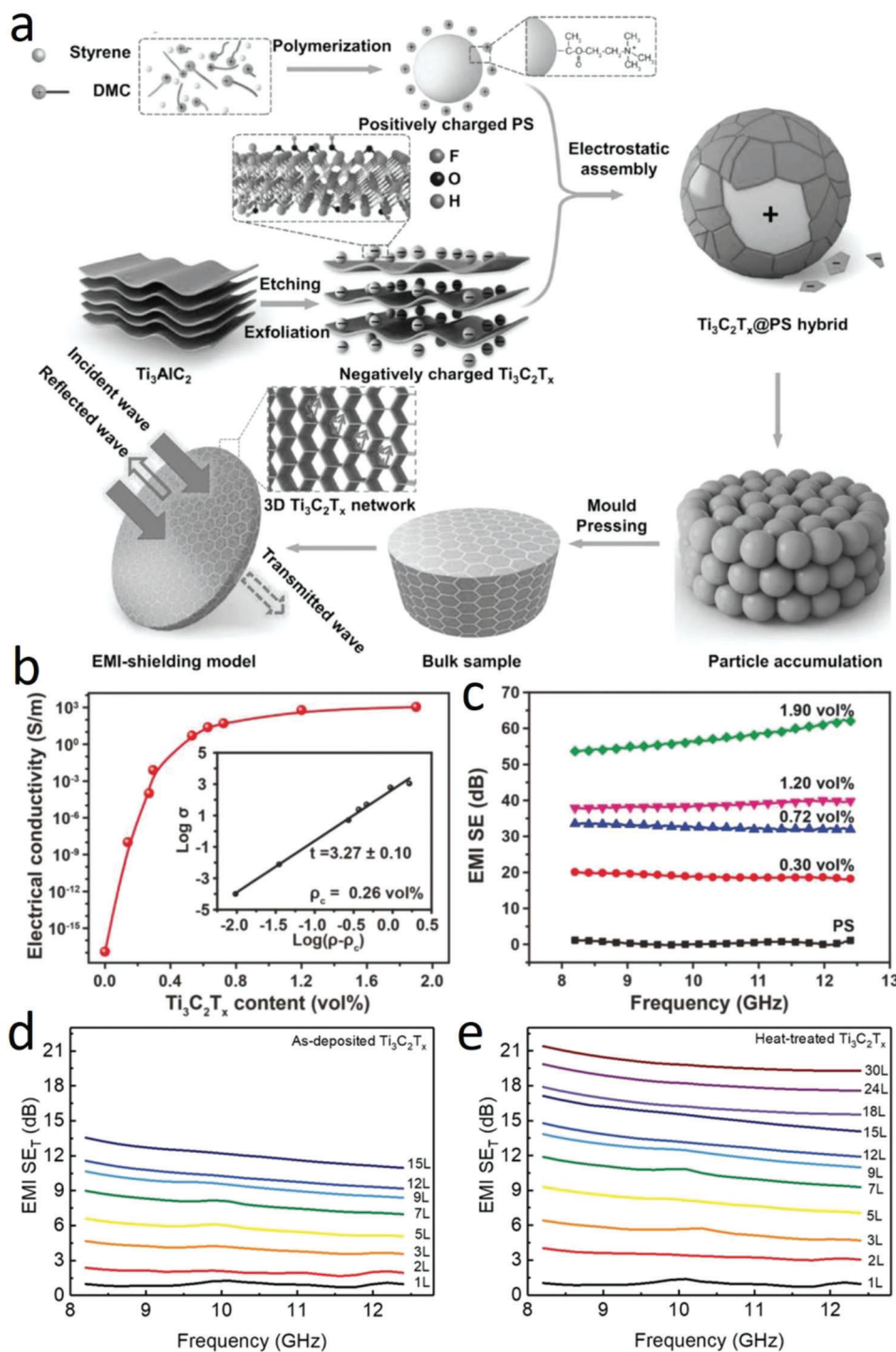


Figure 10. a) Schematic illustrating the fabrication of $\text{Ti}_3\text{C}_2\text{T}_x/\text{PS}$ nanocomposites. b) Plot of electrical conductivity versus MXene content for $\text{Ti}_3\text{C}_2\text{T}_x/\text{PS}$. c) Effect of MXene content on EMI SE of $\text{Ti}_3\text{C}_2\text{T}_x/\text{PS}$. Reproduced with permission.^[143] Copyright 2017, Wiley-VCH. d,e) EMI SE values before and after annealing at 400°C , respectively. Reproduced with permission.^[146] Copyright 2020, Wiley-VCH.

3.6. Solution Casting Method

Solution casting is another method employed in the production of layered MXene composites and requires the preparation of a solution containing the MXene which is then cast

onto a substrate, resulting in a uniform film. Ultraflexible MXene/waterborne PU (WPU) composite films were prepared, which revealed outstanding mechanical strength and electrical conductivity.^[147] From an extremely wide range of MXene contents (10–70 wt%), the EMI SE can be controlled over a broad

Table 5. EMI shielding properties in the X-band of MXene materials produced by different self-assembly methods.

Composition	Method	Thickness [μm]	Conductivity [S cm^{-1}]	EMI SE [dB]	SSE/ t [$\text{dB cm}^2 \text{g}^{-1}$]	Refs.
PPy-modified $\text{Ti}_3\text{C}_2\text{T}_x$ @PET textile	LbL	1300	10	≈ 90	—	[135]
$\text{Ti}_3\text{C}_2\text{T}_x/\text{AgNW}$ @silk fabric		480	$0.8 \Omega \text{sq}^{-1}$	≈ 90	—	[138]
$\text{Ti}_3\text{C}_2\text{T}_x/\text{GO}/\text{cellulose}$		36	412.4	71	18 837.5	[139]
$\text{Ti}_3\text{C}_2\text{T}_x/\text{PI}$		1500	—	62.5	8 567	[140]
$\text{Ti}_3\text{C}_2\text{T}_x/\text{CNT}$		6	—	49	128 680	[141]
$\text{Ti}_3\text{C}_2\text{T}_x/\text{chitosan}$		35	9.69	40.8	10 650	[132]
$\text{Ti}_3\text{C}_2\text{T}_x$ @PANI/PP foam bead		20 000	—	39.8	—	[79]
$\text{Ti}_3\text{C}_2\text{T}_x/\text{PEI-APP}$ @cotton fabric		—	6.7	31.0	—	[136]
PANI/ $\text{Ti}_3\text{C}_2\text{T}_x$ @CF		550	0.2457	26.0	135.5	[133]
$\text{Ti}_3\text{C}_2\text{T}_x/\text{PEI}$ @cotton fabric		0.5 ^{a)}	$11.8 \Omega \text{sq}^{-1}$	20.1	—	[134]
$\text{Ti}_3\text{C}_2\text{T}_x/\text{PA}/\text{PANI}/\text{CNT}$ @cotton fabric		b)	1.42	21	—	[137]
$\text{Ti}_3\text{C}_2\text{T}_x$ -PVA/CNT		0.2	130	2.9	58 187	[131]
$\text{Ti}_3\text{C}_2\text{T}_x/\text{PS}$	Electrostatic	2000	10.81	62	—	[143]
$\text{Ti}_3\text{C}_2\text{T}_x/\text{rGO}$		15	1958	≈ 54.4	27 897	[145]
$\text{Ti}_3\text{C}_2\text{T}_x$ -rGO/PMMA		2000	10.5	> 50	—	[144]
24-layer $\text{Ti}_3\text{C}_2\text{T}_x$	Interfacial	0.055	—	20	—	[146]

^{a)} Thickness of the conductive coating; ^{b)} 20 bilayers of coatings; Ppy—polypyrrole; PET—polyethylene terephthalate; PEI—polyethyleneimine; APP—ammonium polyphosphate; PA—phytic acid; PANI—polyaniline; CNC—cellulose nanocrystals; CF—carbon fiber fabric; AgNW—silver nanowires; GO—graphene oxide; PI—polyimide; CNT—carbon nanotubes; PVA—poly(vinyl alcohol); CNT—carbon nanotubes; PS—polystyrene; PMMA—poly(methyl methacrylate); rGO—reduced graphene oxide.

range. The best performance in the X-band was achieved by a composite containing 70 wt% of MXene with an electric conductivity of 6.63 S cm^{-1} . The EMI SE was about 45.3 dB at a thickness of $510 \mu\text{m}$ for such a composite. Moreover, the composite achieved SE values of more than 34.5 dB in the broadband GHz frequency range, including X-band (8–12 GHz), K_u -band (12–18 GHz), K-band (18–27 GHz), and R-band (27–40 GHz). Annealed $\text{Ti}_3\text{C}_2\text{T}_x/\text{epoxy}$ ^[148] and $\text{Ti}_3\text{C}_2\text{T}_x/\text{PVA}$ ^[149] are examples of other composites prepared by solution casting with an EMI SE in the range of 40–44 dB in the X-band, but differences in the fabrication procedure led to different structures. While in the preparation of the annealed $\text{Ti}_3\text{C}_2\text{T}_x/\text{epoxy}$, the MXene and epoxy were cured together to obtain a composite with $2000 \mu\text{m}$ in thickness,^[148] the repeat casting of PVA and MXene in a succession of 11 cycles led to a $27 \mu\text{m}$ multilayered composite. The MXene content ranged from 15 ($\text{Ti}_3\text{C}_2\text{T}_x/\text{epoxy}$) to 19.5 wt% ($\text{Ti}_3\text{C}_2\text{T}_x/\text{PVA}$) so that it can be said that there is better control over the thickness and structure of the composite with the alternating cast of the different composite constituents which can be useful for thickness tuning. Such a thickness tuning was investigated in MXene/Ni chain/PVDF composites;^[150] for a composite with the same amount of $\text{Ti}_3\text{C}_2\text{T}_x$ and Ni, i.e., 10 wt%, the increase in thickness from 100 to $360 \mu\text{m}$ course to an enhancement of the EMI SE from 19.3 to 34.4 dB. These EMI SE values are higher than using Ni or MXene alone, further evidence that synergetic effects between both conductive and magnetic fillers promote good impedance matching ratio and electrical conductivity. The same synergistic trend was observed in the MXene/Ni hybrids prepared in paraffin by Liang et al.^[151] These composites were prepared by a different method—a one-step hydrothermal process—and, comparing the EMI shielding performance when the same amounts of MXene and Ni are used (10 + 10 wt%), the EMI SE < 10 dB, being another evidence that the solution cast-

ing method is an effective process in the production of layered MXene composites for EMI shielding applications. Also, cellulose nanocrystal-MXene composites were produced by solution casting with good performance at lower thicknesses compared to the research works mentioned in above. The nanocomposites showed EMI SE values of 30–66 dB at thicknesses of ≈ 2 – $14 \mu\text{m}$, resulting in ultrahigh SSE, values of $54\,125 \text{ dB cm}^2 \text{g}^{-1}$.^[152] These achievements were attributed to the synergy effect between the ultrafine cellulose and MXene, which generated abundant interfaces and allowed an excellent conduction and polarization losses.

Table 6 summarizes the EMI shielding performance in the X-band of MXene composites produced by solution casting.

4. Summary and Perspectives

There is no doubt about the importance of the investigation of EMI shielding materials as it is a crucial aspect of ensuring the proper functioning of modern electronic devices. Without effective shielding, these devices are vulnerable to interference, which can result in reduced performance, data loss, and even damage to the devices and health consequences for humans.

Electric conductivity, their ability to absorb or reflect EMW, cost, and availability are the factors considered in the development of EMI shielding materials, and MXenes have shown great interest (Figure 11a) in this area. Among the diversity of MXene composition, the $\text{Ti}_3\text{C}_2\text{T}_x$ MXene is currently the most widely investigated material for EMI shielding (Figure 11b), making it a well-understood and reliable material but other MXenes such as Ti_3CNT_x ^[37] and V_2CT_x ^[10] have also shown potential as a shield. Regardless of the excellent EMI shielding performance of MXene materials, properties like lightweight and mechanical flexibility are highly desired.

Table 6. EMI shielding properties in the X-band of MXene films produced by solution casting.

Composition ^{a)}	Method	Structure design	Thickness [μm]	Conductivity [S cm^{-1}]	EMI SE [dB]	SSE/ t [$\text{dB cm}^2 \text{g}^{-1}$]	Refs.
$\text{Ti}_3\text{C}_2\text{T}_x/\text{CNC}$	Solution casting	Brick and mortar	14	≈ 1000	66	54 125	[152]
$\text{Ti}_3\text{C}_2\text{T}_x/\text{WPU}$		Multilayered	510	6.63	45.3	—	[147]
$\text{Ti}_3\text{C}_2\text{T}_x/\text{PVA}$			27	7.16	44.4	9 343	[149]
$\text{Ti}_3\text{C}_2\text{T}_x/\text{epoxy}$		Porous	2000	1.05	41	—	[148]
$\text{Ti}_3\text{C}_2\text{T}_x/\text{Ni}/\text{PVDF}$		Multilayered	360	—	34.4	—	[150]

^{a)} CNC—cellulose nanocrystals; WPU—waterborne polyurethane; PVA—poly(vinyl alcohol); PVDF—polyvinylidene fluoride.

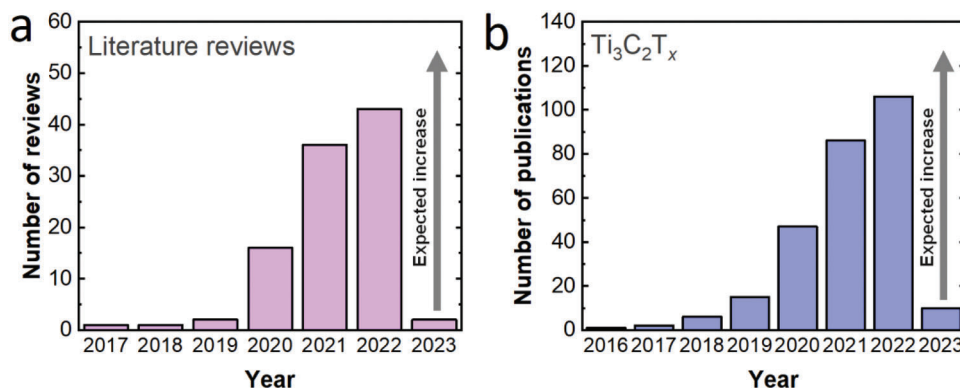


Figure 11. a) The number of literature reviews focused on MXenes for EMI shielding (source: Scopus, December 2022). b) The number of research publications focused on $\text{Ti}_3\text{C}_2\text{T}_x$ MXene with EMI shielding properties (source: Scopus, December 2022).

Composites with thermal stability and resistance are also needed not only because certain processing techniques require the use of high thermal temperatures, but also because of the temperatures to which composites potentially applied in the aeronautics and aerospace industries may be subjected. To achieve that, the most common strategy is to mix MXenes with a polymer matrix to form a composite. Different categories of polymers are found in the preparation of MXene-polymer composites such as i) engineering polymers such as aramid, PS, PVDF, PDMS, PU; ii) intrinsic conductive polymers that include PANI, PPy, PEDOT: PSS; iii) natural and biodegradable polymers such as chitosan, cellulose, NR and PVA; and iv) high-performance polymers for thermoelectric properties like PI. The obtaining of all these compositions requires the use of different processing techniques such as vacuum-filtration, freeze-drying, and foaming methods, printing techniques, electrospinning, self-assembly, and solution casting methods. The main difference between these techniques for obtaining MXene shielding materials lies in how the MXene is manipulated. For instance, by electrospinning, a solution or suspension of MXene NS can be drawn into a thin fiber by applying an electric field to create MXene-based fibers or membranes with high surface area and high aspect ratio. While an MXene aerogel is produced by freeze-drying to create a lightweight and porous material. However, all these processes have in common that they require optimization of parameters such as the amount of filler, thickness of the final product, and potential chemical modifications. These have a significant impact on the performance of the potential shield material, particularly in the electric conductivity which is a critical factor for effective EMI shielding. Another important reason is the optimization of the mentioned parameters

that can affect the flexibility, durability, and chemical resistance of the MXene material. This could enhance performance and required properties for applicable devices like wearable electronics.

Aside from the need for an EMI shielding effect that has been well demonstrated by MXenes, the need arises to achieve EMI shielding through an absorption mechanism. The reflection mechanism of EMI shielding can be useful for certain applications such as radar systems where reflected EMW are used to determine the distance and location of objects. However, it can simultaneously damage electronic devices by EMI, the effect of which is currently to be avoided when investigating new materials in this area. Therefore, it is important to use EMI shielding materials that can effectively absorb or dissipate the EMW. EMI shielding through absorption involves the use of materials that absorb and dissipate EMW to reduce their intensity or prevent them from passing through the shielding material. In the mechanism behind EMI shielding by absorption, the following properties are desired: i) high electrical conductivity for ohmic loss, resulting in enhanced interaction between the high electron density and the incident EMW, ii) electric dipoles provided by dielectric materials with a high dielectric constant are desired for dielectric loss, and iii) magnetic dipoles for a large magnetic permeability which leads to magnetic loss. Many current literatures have been considering the values of SE_R or SE_A to classify the predominant EMI shielding mechanism in a shield. However, power coefficients R and A , provide a more complete picture of a material interacting with EMW and as seen in this review work, this approach was considered only in a few reports.^[70,71,79,88,118]

Moreover, the concepts of the green shielding material and green shielding index^[28] were also introduced to classify a ma-

terial that absorbs most of the incident EMW. However, this classification has not been used since the MXene materials mostly have a reflection shielding effect. This predominant reflection mechanism may be because most of the produced MXene materials are $Ti_3C_2T_x$ -based MXenes which are electrically conductive and result in increased impedance mismatch at the interface between air and MXene surface, thus, a high R value. The reduction of reflection may lie in the combination a gradient conductive network and a foam structure as successful demonstrated with the production of MXene-decorated polymer foam beads with an ultralow R coefficient of ≈ 0.05 .^[79] Layered V_2CT_x and $V_4C_3T_x$ also exhibited efficient EMW absorption in the whole X-band when incorporated into a PU matrix with ultralow mass loadings (≈ 2 wt%)^[153] suggesting vanadium-based MXenes as promising EMW absorbers. However, the development of MXene-shielding materials with EMW absorption properties is still in its infancy.

In the preparation of MXenes, their oxidation resistance remains a challenge. MXenes are highly susceptible to oxidative degradation, which deteriorates their unique properties and decreases their EMI shielding performance. This poor oxidative resistance of MXenes can be addressed by controlling various presynthesis and postsynthesis parameters, including the quality of the MAX phase precursors and etching procedures. For instance, the use of a water-free etching process can allow for the control of the terminals of the MXenes ($-T_x$), which have an impact on the electrical properties of MXenes, and consequently, on the attenuation of EMW. In order to avoid performing dilute investigations on different MXenes, researchers should devote more emphasis to computational modeling. This can be used to optimize the design of MXene-based materials for EMI shielding applications and to predict their properties and performance. Besides the improvement as a potential shield, computational methods could also be useful in predicting mechanical properties, thereby addressing another current challenge in the preparation of MXene-based composites. Mechanical properties can impact the overall performance and reliability of the potential composite for EMI shielding and should be considered in the design of the shield, particularly in applications that require high mechanical strength and durability, such as aerospace and defense applications or even consumer electronics applications that are subject to frequent use and must be able to withstand mechanical stresses such as dropping, bending, and twisting. In this framework, the use of polymer matrices can significantly improve the mechanical properties of MXene-based composites, making them more durable and reliable for EMI shielding applications. By incorporating MXenes into a polymer matrix, the resulting composite can take advantage of the unique properties of MXenes, such as their high EMI shielding performance, while also benefiting from the mechanical strength and flexibility of the polymer matrix. Additionally, the use of a polymer matrix can also improve the oxidative resistance of MXenes by providing a protective barrier against oxidation. This can help to mitigate the challenges associated with the poor oxidative resistance of MXenes and improve the overall performance and longevity of MXene-based composites for EMI shielding applications.

The scalability of MXene-shielding materials in the industry is another aspect that must be considered. In addition to the fact that one of the challenges in MXenes is that their synthesis is cur-

rently limited to small batch sizes, which can be time-consuming and costly, more sustainable processes are also needed. Most of the MXenes are still synthesized using HF or generating in situ HF, thus urgent to employ clean and green chemistry synthesis protocols. In terms of processing techniques, there are still challenges that need to be addressed in terms of efficiency, cost, and scalability. In this regard, expanding research groups are suggested to innovate scalable techniques and make such processes of LbL, vacuum filtration, and freeze-drying methods more practical for synthesizing MXenes with a viable option for widespread use in industry. Thus, the full potential of MXene materials as an EMI shield will be applied in the real world. In fact, more attention should be paid to freeze-drying and foaming methods, electrospinning, and 3D printing processes. Freeze-drying and foaming methods offer an opportunity to create materials with low density, large porosity, and high specific surface area. These characteristics are particularly important in sectors where weight reduction is essential, such as aircraft and portable electronic devices. Moreover, porous structures have particular relevance in higher absorption of EMW by providing several interfaces for multiple scattering and polarization effects. Electrospinning is important for producing wearable and portable electronic EMI shielding materials. Many industrial companies have been using this process to manufacture electrospun fibers which can allow a smoother implementation of MXenes in the process. 3D printing enables the rapid production of custom-shaped and highly effective EMI shielding materials with tailored properties in any situation and environment. This can be a huge advantage for specific niches like military applications.

Finally, from an industrial perspective, it seems relevant to consider Life Cycle Assessment (LCA) and Environmental Risk Assessment (ERA) for evaluating the environmental impacts and potential risks of the MXene-shielding materials throughout their entire life cycle, from raw material to manufacturing, distribution, use, recycling, and final disposal. These assessments will help the development of more sustainable and environmentally-friendly production methods and identify any potential risks that need to be addressed. With ERA, potential risks to human health and other living organisms, and the environment from the use of MXenes and other conductive and/or magnetic fillers used in the final product such as the release of toxic substances or the potential for environmental contamination should be considered. All this information, together with a strong knowledge base about MXenes, including their characterization and synthesis, will guide decision-making and ensure that MXene-shielding materials are developed and used responsibly and sustainably, thus protecting us and next-generation electronic devices from the harm of EMW.

Acknowledgements

This work was supported by the ERC-CZ program (Project No. LL2101) and CHEMFELLS V (Project No. CZ.02.01.01/00/22_010/0003004) from the Ministry of Education Youth and Sports (MEYS).

Conflict of Interest

The authors declare no conflict of interest.

Keywords

2D materials, electromagnetic interference shielding, green shielding materials, MXenes, power coefficients, processing strategies

Received: January 28, 2023

Revised: April 7, 2023

Published online:

- [1] J.-M. Thomassin, C. Jérôme, T. Pardoën, C. Bailly, I. Huynen, C. De-trembleur, *Mater. Sci. Eng., R* **2013**, *74*, 211.
- [2] M.-S. Cao, Y.-Z. Cai, P. He, J.-C. Shu, W.-Q. Cao, J. Yuan, *Chem. Eng. J.* **2019**, *359*, 1265.
- [3] H. Abbasi, M. Antunes, J. I. Velasco, *Prog. Mater. Sci.* **2019**, *103*, 319.
- [4] A. Iqbal, P. Sambyal, C. M. Koo, *Adv. Funct. Mater.* **2020**, *30*, 2000883.
- [5] D. W. Hatchett, M. Josowicz, *Chem. Rev.* **2008**, *108*, 746.
- [6] J. Kruželák, A. Kvasničáková, K. Hložeková, I. Hudec, *Nanoscale Adv.* **2021**, *3*, 123.
- [7] Z. Fu, N. Wang, D. Legut, C. Si, Q. Zhang, S. Du, T. C. Germann, J. S. Francisco, R. Zhang, *Chem. Rev.* **2019**, *119*, 11980.
- [8] A. Kamshyn, S. Magdassi, *Chem. Soc. Rev.* **2019**, *48*, 1712.
- [9] F. Shahzad, M. Alhabeab, C. B. Hatter, B. Anasori, S. Man Hong, C. M. Koo, Y. Gogotsi, *Science* **2016**, *353*, 1137.
- [10] M. Han, C. E. Shuck, R. Rakhmanov, D. Parchment, B. Anasori, C. M. Koo, G. Friedman, Y. Gogotsi, *ACS Nano* **2020**, *14*, 5008.
- [11] J. Liu, H.-B. Zhang, R. Sun, Y. Liu, Z. Liu, A. Zhou, Z.-Z. Yu, *Adv. Mater.* **2017**, *29*, 1702367.
- [12] M. Han, X. Yin, H. Wu, Z. Hou, C. Song, X. Li, L. Zhang, L. Cheng, *ACS Appl. Mater. Interfaces* **2016**, *8*, 21011.
- [13] M. Naguib, M. Kurtoglu, V. Presser, J. Lu, J. Niu, M. Heon, L. Hultman, Y. Gogotsi, M. W. Barsoum, *Adv. Mater.* **2011**, *23*, 4248.
- [14] G. Deysher, C. E. Shuck, K. Hantanasirisakul, N. C. Frey, A. C. Foucher, K. Maleski, A. Sarycheva, V. B. Shenoy, E. A. Stach, B. Anasori, Y. Gogotsi, *ACS Nano* **2020**, *14*, 204.
- [15] B. C. Wyatt, A. Rosenkranz, B. Anasori, *Adv. Mater.* **2021**, *33*, 2007973.
- [16] J. Gonzalez-Julian, *J. Am. Ceram. Soc.* **2021**, *104*, 659.
- [17] X. Jiang, A. V. Kuklin, A. Baev, Y. Ge, H. Ågren, H. Zhang, P. N. Prasad, *Phys. Rep.* **2020**, *848*, 1.
- [18] L. Verger, V. Natu, M. Carey, M. W. Barsoum, *Trends Chem.* **2019**, *1*, 656.
- [19] B. Anasori, M. R. Lukatskaya, Y. Gogotsi, *Nat. Rev. Mater.* **2017**, *2*, 16098.
- [20] Y. Gogotsi, B. Anasori, *ACS Nano* **2019**, *13*, 8491.
- [21] Y. Gogotsi, Q. Huang, *ACS Nano* **2021**, *15*, 5775.
- [22] M. Naguib, M. W. Barsoum, Y. Gogotsi, *Adv. Mater.* **2021**, *33*, 2103393.
- [23] M. S. Bhargava Reddy, S. Kailasa, B. C. G. Marupalli, K. K. Sadasivuni, S. Aich, *ACS Sens.* **2022**, *7*, 2132.
- [24] S. K. Nemani, B. Zhang, B. C. Wyatt, Z. D. Hood, S. Manna, R. Khale-dialidusti, W. Hong, M. G. Sternberg, S. K. R. S. Sankaranarayanan, B. Anasori, *ACS Nano* **2021**, *15*, 12815.
- [25] Z. Du, C. Wu, Y. Chen, Z. Cao, R. Hu, Y. Zhang, J. Gu, Y. Cui, H. Chen, Y. Shi, J. Shang, B. Li, S. Yang, *Adv. Mater.* **2021**, *33*, 2101473.
- [26] J. Zhou, Q. Tao, B. Ahmed, J. Palisaitis, I. Persson, J. Halim, M. W. Barsoum, P. O. Å. Persson, J. Rosen, *Chem. Mater.* **2022**, *34*, 2098.
- [27] Z. Du, C. Wu, Y. Chen, Q. Zhu, Y. Cui, H. Wang, Y. Zhang, X. Chen, J. Shang, B. Li, W. Chen, C. Liu, S. Yang, *Adv. Energy Mater.* **2022**, *12*, 2103228.
- [28] X.-X. Wang, J.-C. Shu, W.-Q. Cao, M. Zhang, J. Yuan, M.-S. Cao, *Chem. Eng. J.* **2019**, *369*, 1068.
- [29] J. Cheng, C. Li, Y. Xiong, H. Zhang, H. Raza, S. Ullah, J. Wu, G. Zheng, Q. Cao, D. Zhang, Q. Zheng, R. Che, *Nano-Micro Lett.* **2022**, *14*, 80.
- [30] X. Jia, Y. Li, B. Shen, W. Zheng, *Composites, Part B* **2022**, *233*, 109652.
- [31] H. W. Ott, in *Electromagnetic Compatibility Engineering* (Ed: H. W. Ott), Wiley, NJ **2009**, pp. 238–301.
- [32] R. Schmitt, in *Electromagnetic Explain* (Ed: R. Schmitt), Newnes, Burlington **2002**, pp. 181–207.
- [33] V. Shukla, *Nanoscale Adv.* **2019**, *1*, 1640.
- [34] F. M. Oliveira, R. Gusmão, *ACS Appl. Electron. Mater.* **2020**, *2*, 3048.
- [35] F. M. Oliveira, J. Luxa, D. Bouša, Z. Sofer, R. Gusmão, *ACS Appl. Nano Mater.* **2022**, *5*, 6792.
- [36] Department of Defense Washington DC, in *Military Handbook – Grounding, Bonding Shielding for Electronic Equipments and Facilities, Vol. 1*, Department of Defense, Washington DC **1987**, pp. 1–80.
- [37] A. Iqbal, F. Shahzad, K. Hantanasirisakul, M.-K. Kim, J. Kwon, J. Hong, H. Kim, D. Kim, Y. Gogotsi, C. M. Koo, *Science* **2020**, *369*, 446.
- [38] J. Liu, Z. Liu, H.-B. Zhang, W. Chen, Z. Zhao, Q.-W. Wang, Z.-Z. Yu, *Adv. Electron. Mater.* **2020**, *6*, 1901094.
- [39] B. Zhou, Y. Li, Z. Li, J. Ma, K. Zhou, C. Liu, C. Shen, Y. Feng, *J. Mater. Chem. C* **2021**, *9*, 10425.
- [40] L. Li, Y. Cao, X. Liu, J. Wang, Y. Yang, W. Wang, *ACS Appl. Mater. Interfaces* **2020**, *12*, 27350.
- [41] Y. Zhang, W. Cheng, W. Tian, J. Lu, L. Song, K. M. Liew, B. Wang, Y. Hu, *ACS Appl. Mater. Interfaces* **2020**, *12*, 6371.
- [42] R. Liu, M. Miao, Y. Li, J. Zhang, S. Cao, X. Feng, *ACS Appl. Mater. Interfaces* **2018**, *10*, 44787.
- [43] Y. Zhang, L. Wang, J. Zhang, P. Song, Z. Xiao, C. Liang, H. Qiu, J. Kong, J. Gu, *Compos. Sci. Technol.* **2019**, *183*, 107833.
- [44] M. Yang, K. Cao, L. Sui, Y. Qi, J. Zhu, A. Waas, E. M. Arruda, J. Kieffer, M. D. Thouless, N. A. Kotov, *ACS Nano* **2011**, *5*, 6945.
- [45] F. Xie, F. Jia, L. Zhuo, Z. Lu, L. Si, J. Huang, M. Zhang, Q. Ma, *Nanoscale* **2019**, *11*, 23382.
- [46] C. Weng, T. Xing, H. Jin, G. Wang, Z. Dai, Y. Pei, L. Liu, Z. Zhang, *Composites, Part A* **2020**, *135*, 105927.
- [47] Z. Ma, S. Kang, J. Ma, L. Shao, Y. Zhang, C. Liu, A. Wei, X. Xiang, L. Wei, J. Gu, *ACS Nano* **2020**, *14*, 8368.
- [48] J. Lu, L. Cheng, C. Liao, P. Jia, L. Song, B. Wang, Y. Hu, *Adv. Mater. Interfaces* **2022**, *9*, 2101359.
- [49] F. Liu, Y. Li, S. Hao, Y. Cheng, Y. Zhan, C. Zhang, Y. Meng, Q. Xie, H. Xia, *Carbohydr. Polym.* **2020**, *243*, 116467.
- [50] J.-Q. Luo, S. Zhao, H.-B. Zhang, Z. Deng, L. Li, Z.-Z. Yu, *Compos. Sci. Technol.* **2019**, *182*, 107754.
- [51] H. Wu, C. Zhu, X. Li, X. Hu, H. Xie, X. Lu, J.-P. Qu, *Macromol. Rapid Commun.* **2022**, *43*, 2200387.
- [52] S. C. Tjong, *Mater. Sci. Eng., R* **2006**, *53*, 73.
- [53] Y. Zare, *Composites, Part A* **2016**, *84*, 158.
- [54] W.-T. Cao, F.-F. Chen, Y.-J. Zhu, Y.-G. Zhang, Y.-Y. Jiang, M.-G. Ma, F. Chen, *ACS Nano* **2018**, *12*, 4583.
- [55] B. Zhou, Z. Zhang, Y. Li, G. Han, Y. Feng, B. Wang, D. Zhang, J. Ma, C. Liu, *ACS Appl. Mater. Interfaces* **2020**, *12*, 4895.
- [56] M. Zhu, X. Yan, H. Xu, Y. Xu, L. Kong, *Ceram. Int.* **2021**, *47*, 17234.
- [57] W. Cao, C. Ma, S. Tan, M. Ma, P. Wan, F. Chen, *Nano-Micro Lett.* **2019**, *11*, 72.
- [58] K. Qian, H. Wu, J. Fang, Y. Yang, M. Miao, S. Cao, L. Shi, X. Feng, *Carbohydr. Polym.* **2021**, *254*, 117325.
- [59] W. Xin, G.-Q. Xi, W.-T. Cao, C. Ma, T. Liu, M.-G. Ma, J. Bian, *RSC Adv.* **2019**, *9*, 29636.
- [60] B. Zhou, Q. Li, P. Xu, Y. Feng, J. Ma, C. Liu, C. Shen, *Nanoscale* **2021**, *13*, 2378.
- [61] F. Zhang, P. Ren, Z. Guo, J. Wang, Z. Chen, Z. Zong, J. Hu, Y. Jin, F. Ren, *J. Mater. Sci. Technol.* **2022**, *129*, 181.
- [62] C. Ma, W.-T. Cao, W. Zhang, M.-G. Ma, W.-M. Sun, J. Zhang, F. Chen, *Chem. Eng. J.* **2021**, *403*, 126438.

- [63] D. Liu, Y. Gao, Y. Song, H. Zhu, L. Zhang, Y. Xie, H. Shi, Z. Shi, Q. Yang, C. Xiong, *Biomacromolecules* **2022**, *23*, 182.
- [64] M. Miao, R. Liu, S. Thaiboonrod, L. Shi, S. Cao, J. Zhang, J. Fang, X. Feng, *J. Mater. Chem. C* **2020**, *8*, 3120.
- [65] X. Jia, B. Shen, L. Zhang, W. Zheng, *Composites, Part B* **2020**, *198*, 108250.
- [66] K. Qian, Q. Zhou, H. Wu, J. Fang, M. Miao, Y. Yang, S. Cao, L. Shi, X. Feng, *Composites, Part A* **2021**, *141*, 106229.
- [67] Y. Wang, R. Liu, J. Zhang, M. Miao, X. Feng, *Appl. Surf. Sci.* **2021**, *546*, 149143.
- [68] K. Qian, S. Li, J. Fang, Y. Yang, S. Cao, M. Miao, X. Feng, *J. Mater. Sci. Technol.* **2022**, *127*, 71.
- [69] A. Iqbal, P. Sambyal, J. Kwon, M. Han, J. Hong, S. J. Kim, M.-K. Kim, Y. Gogotsi, C. M. Koo, *Compos. Sci. Technol.* **2021**, *213*, 108878.
- [70] P. He, M.-S. Cao, Y.-Z. Cai, J.-C. Shu, W.-Q. Cao, J. Yuan, *Carbon* **2020**, *157*, 80.
- [71] M. Ma, W. Tao, X. Liao, S. Chen, Y. Shi, H. He, X. Wang, *Chem. Eng. J.* **2023**, *452*, 139471.
- [72] S. Gong, X. Sheng, X. Li, M. Sheng, H. Wu, X. Lu, J. Qu, *Adv. Funct. Mater.* **2022**, *32*, 2200570.
- [73] R. Bian, G. He, W. Zhi, S. Xiang, T. Wang, D. Cai, *J. Mater. Chem. C* **2019**, *7*, 474.
- [74] M. Han, X. Yin, K. Hantanasirisakul, X. Li, A. Iqbal, C. B. Hatter, B. Anasori, C. M. Koo, T. Torita, Y. Soda, L. Zhang, L. Cheng, Y. Gogotsi, *Adv. Opt. Mater.* **2019**, *7*, 1900267.
- [75] S. Zhao, H.-B. Zhang, J.-Q. Luo, Q.-W. Wang, B. Xu, S. Hong, Z.-Z. Yu, *ACS Nano* **2018**, *12*, 11193.
- [76] Z. Zeng, C. Wang, G. Siqueira, D. Han, A. Huch, S. Abdolhosseinzadeh, J. Heier, F. Nüesch, C. (John) Zhang, G. Nyström, *Adv. Sci.* **2020**, *7*, 2000979.
- [77] N. Wu, Y. Yang, C. Wang, Q. Wu, F. Pan, R. Zhang, J. Liu, Z. Zeng, *Adv. Mater.* **2023**, *35*, 2207969.
- [78] X. Wu, B. Han, H.-B. Bin Zhang, X. Xie, T. Tu, Y. Zhang, Y. Dai, R. Yang, Z.-Z. Z. Yu, *Chem. Eng. J.* **2020**, *381*, 122622.
- [79] X. Jia, B. Shen, L. Zhang, W. Zheng, *Carbon* **2021**, *173*, 932.
- [80] Y. Wang, Q. Qi, G. Yin, W. Wang, D. Yu, *ACS Appl. Mater. Interfaces* **2021**, *13*, 21831.
- [81] J. Liu, H.-B. Zhang, X. Xie, R. Yang, Z. Liu, Y. Liu, Z.-Z. Yu, *Small* **2018**, *14*, 1802479.
- [82] P. Sambyal, A. Iqbal, J. Hong, H. Kim, M.-K. Kim, S. M. Hong, M. Han, Y. Gogotsi, C. M. Koo, *ACS Appl. Mater. Interfaces* **2019**, *11*, 38046.
- [83] Z. Deng, P. Tang, X. Wu, H.-B. Zhang, Z.-Z. Yu, *ACS Appl. Mater. Interfaces* **2021**, *13*, 20539.
- [84] Z. Zhou, J. Liu, X. Zhang, D. Tian, Z. Zhan, C. Lu, *Adv. Mater. Interfaces* **2019**, *6*, 1802040.
- [85] H. Liu, Z. Huang, T. Chen, X. Su, Y. Liu, R. Fu, *Chem. Eng. J.* **2022**, *427*, 131540.
- [86] Y. Yang, B. Li, N. Wu, W. Liu, S. Zhao, C. J. Zhang, J. Liu, Z. Zeng, *ACS Mater. Lett.* **2022**, *4*, 2352.
- [87] Y. Yang, N. Wu, B. Li, W. Liu, F. Pan, Z. Zeng, J. Liu, *ACS Nano* **2022**, *16*, 15042.
- [88] H. Xu, X. Yin, X. Li, M. Li, S. Liang, L. Zhang, L. Cheng, *ACS Appl. Mater. Interfaces* **2019**, *11*, 10198.
- [89] Y.-Z. Zhang, Y. Wang, Q. Jiang, J. K. El-Demellawi, H. Kim, H. N. Alshareef, *Adv. Mater.* **2020**, *32*, 1908486.
- [90] L. Wu, Z. Dong, F. Li, H. Zhou, Y. Song, *Adv. Opt. Mater.* **2016**, *4*, 1915.
- [91] M. Vural, A. Pena-Francesch, J. Bars-Pomes, H. Jung, H. Gudapati, C. B. Hatter, B. D. Allen, B. Anasori, I. T. Ozbolat, Y. Gogotsi, M. C. Demirel, *Adv. Funct. Mater.* **2018**, *28*, 1801972.
- [92] H. Wu, Y. Xie, Y. Ma, B. Zhang, B. Xia, P. Zhang, W. Qian, D. He, X. Zhang, B.-W. Li, C.-W. Nan, *Small* **2022**, *18*, 2107087.
- [93] Z. Deng, L. Li, P. Tang, C. Jiao, Z.-Z. Yu, C. M. Koo, H.-B. Zhang, *ACS Nano* **2022**, *16*, 16976.
- [94] S. Zhou, G. Zhang, Z. Nie, H. Liu, H. Yu, Y. Liu, K. Bi, W. Geng, H. Duan, X. Chou, *Mater. Chem. Front.* **2022**, *6*, 1736.
- [95] X. Wu, T. Tu, Y. Dai, P. Tang, Y. Zhang, Z. Deng, L. Li, H.-B. Zhang, Z.-Z. Yu, *Nano-Micro Lett.* **2021**, *13*, 148.
- [96] Y. Dai, X. Wu, L. Li, Y. Zhang, Z. Deng, Z.-Z. Yu, H.-B. Zhang, *J. Mater. Chem. A* **2022**, *10*, 11375.
- [97] C.-Z. Qi, X. Wu, J. Liu, X.-J. Luo, H.-B. Zhang, Z.-Z. Yu, *J. Mater. Sci. Technol.* **2023**, *135*, 213.
- [98] L. Li, Z. Deng, M. Chen, Z.-Z. Yu, T. P. Russell, H.-B. Zhang, *Nano Lett.* **2023**, *23*, 155.
- [99] M. Champeau, D. A. Heinze, T. N. Viana, E. R. de Souza, A. C. Chinellato, S. Titotto, *Adv. Funct. Mater.* **2020**, *30*, 1910606.
- [100] Z. Li, D. Feng, B. Li, D. Xie, Y. Mei, *Compos. Sci. Technol.* **2023**, *231*, 109803.
- [101] J. Liu, L. Mckeon, J. Garcia, S. Pinilla, S. Barwich, M. Möbius, P. Stamenov, J. N. Coleman, V. Nicolosi, *Adv. Mater.* **2022**, *34*, 2106253.
- [102] Y. Zhu, J. Liu, T. Guo, J. J. Wang, X. Tang, V. Nicolosi, *ACS Nano* **2021**, *15*, 1465.
- [103] A. Greiner, J. H. Wendorff, *Angew. Chem., Int. Ed.* **2007**, *46*, 5670.
- [104] J. Xue, T. Wu, Y. Dai, Y. Xia, *Chem. Rev.* **2019**, *119*, 5298.
- [105] D. Li, Y. Xia, *Adv. Mater.* **2004**, *16*, 1151.
- [106] J. F. Cooley, US692631A, **1902**.
- [107] W. J. Morton, US705691A, **1902**.
- [108] A. Formhals, US1975504A, **1934**.
- [109] A. Formhals, US1975504, **1939**.
- [110] G. I. Taylor, *Proc. R. Soc. London, Ser. A* **1964**, *280*, 383.
- [111] G. I. Taylor, M. D. Van Dyke, *Proc. R. Soc. London, Ser. A* **1966**, *291*, 145.
- [112] G. I. Taylor, M. D. Van Dyke, *Proc. R. Soc. London, Ser. A* **1969**, *313*, 453.
- [113] P. Martins, A. C. Lopes, S. Lancers-Mendez, *Prog. Polym. Sci.* **2014**, *39*, 683.
- [114] H. Zhang, G. Zhang, Q. Gao, M. Tang, Z. Ma, J. Qin, M. Wang, J.-K. Kim, *Chem. Eng. J.* **2020**, *379*, 122304.
- [115] H. Guo, Y. Chen, Y. Li, W. Zhou, W. Xu, L. Pang, X. Fan, S. Jiang, *Composites, Part A* **2021**, *143*, 106309.
- [116] Y.-R. Zhang, B.-C. Wang, S.-L. Gao, L.-P. Qiu, Q.-H. Zheng, G.-T. Cheng, W.-P. Han, S. Ramakrishna, Y.-Z. Long, *ACS Appl. Nano Mater.* **2022**, *5*, 12320.
- [117] Y. Zhang, K. Ruan, J. Gu, *Small* **2021**, *17*, 2101951.
- [118] L. Liu, R. Guo, J. Gao, Q. Ding, Y. Fan, J. Yu, *Etoiles Compos. Chim. Anorm. Debut Sequence Princ., Commun. Colloq. Int. Astrophys., 23rd* **2022**, *30*, 101094.
- [119] Y. Wang, H.-K. Peng, T.-T. Li, B.-C. Shiu, H.-T. Ren, X. Zhang, C.-W. Lou, J.-H. Lin, *Chem. Eng. J.* **2021**, *412*, 128681.
- [120] Y. Wang, T.-T. Li, B.-C. Shiu, X. Zhang, H.-K. Peng, C.-W. Lou, J.-H. Lin, *J. Mater. Res. Technol.* **2021**, *15*, 6011.
- [121] Y. Wang, T.-T. Li, B.-C. Shiu, X. Zhang, H.-K. Peng, C.-W. Lou, J.-H. Lin, *Appl. Surf. Sci.* **2022**, *574*, 151552.
- [122] Z. Miao, X. Chen, H. Zhou, P. Liu, S. Fu, J. Yang, Y. Gao, Y. Ren, D. Rong, *Nanomaterials* **2022**, *12*, 20.
- [123] C. Cui, C. Xiang, L. Geng, X. Lai, R. Guo, Y. Zhang, H. Xiao, J. Lan, S. Lin, S. Jiang, *J. Alloys Compd.* **2019**, *788*, 1246.
- [124] S. Yang, D.-X. Yan, Y. Li, J. Lei, Z.-M. Li, *Ind. Eng. Chem. Res.* **2021**, *60*, 9824.
- [125] Y. Zhang, Z. Ma, K. Ruan, J. Gu, *Nano Res.* **2022**, *15*, 5601.
- [126] Z. Du, K. Chen, Y. Zhang, Y. Wang, P. He, H.-Y. Mi, Y. Wang, C. Liu, C. Shen, *Etoiles Compos. Chim. Anorm. Debut Sequence Princ., Commun. Colloq. Int. Astrophys., 23rd* **2021**, *26*, 100770.
- [127] W. Yuan, J. Yang, F. Yin, Y. Li, Y. Yuan, *Etoiles Compos. Chim. Anorm. Debut Sequence Princ., Commun. Colloq. Int. Astrophys., 23rd* **2020**, *19*, 90.

- [128] J. Dong, S. Luo, S. Ning, G. Yang, D. Pan, Y. Ji, Y. Feng, F. Su, C. Liu, *ACS Appl. Mater. Interfaces* **2021**, *13*, 60478.
- [129] S. Zhang, J. Wu, J. Liu, Z. Yang, G. Wang, *ACS Appl. Nano Mater.* **2021**, *4*, 13976.
- [130] M. Yang, Z. Yang, C. Lv, Z. Wang, Z. Lu, G. Lu, X. Jia, C. Wang, *Compos. Sci. Technol.* **2022**, *221*, 109313.
- [131] G.-M. Weng, J. Li, M. Alhabeb, C. Karpovich, H. Wang, J. Lipton, K. Maleski, J. Kong, E. Shaulsky, M. Elimelech, Y. Gogotsi, A. D. Taylor, *Adv. Funct. Mater.* **2018**, *28*, 1803360.
- [132] Z. Tan, H. Zhao, F. Sun, L. Ran, L. Yi, L. Zhao, J. Wu, *Composites, Part A* **2022**, *155*, 106809.
- [133] G. Yin, Y. Wang, W. Wang, D. Yu, *Colloids Surf., A* **2020**, *601*, 125047.
- [134] C. Lan, H. Jia, M. Qiu, S. Fu, *ACS Appl. Mater. Interfaces* **2021**, *13*, 38761.
- [135] Q.-W. Wang, H.-B. Zhang, J. Liu, S. Zhao, X. Xie, L. Liu, R. Yang, N. Koratkar, Z.-Z. Yu, *Adv. Funct. Mater.* **2019**, *29*, 1806819.
- [136] W. Cheng, Y. Zhang, W. Tian, J. Liu, J. Lu, B. Wang, W. Xing, Y. Hu, *Ind. Eng. Chem. Res.* **2020**, *59*, 14025.
- [137] Y. Mao, D. Wang, S. Fu, *Composites, Part A* **2022**, *153*, 106751.
- [138] L.-X. Liu, W. Chen, H.-B. Zhang, Q.-W. Wang, F. Guan, Z.-Z. Yu, *Adv. Funct. Mater.* **2019**, *29*, 1905197.
- [139] B. Li, N. Wu, Y. Yang, F. Pan, C. Wang, G. Wang, L. Xiao, W. Liu, J. Liu, Z. Zeng, *Adv. Funct. Mater.* **2023**, *33*, 2213357.
- [140] Z.-H. Zeng, N. Wu, J.-J. Wei, Y.-F. Yang, T.-T. Wu, B. Li, S. B. Hauser, W.-D. Yang, J.-R. Liu, S.-Y. Zhao, *Nano-Micro Lett.* **2022**, *14*, 59.
- [141] B. Li, Y. Yang, N. Wu, S. Zhao, H. Jin, G. Wang, X. Li, W. Liu, J. Liu, Z. Zeng, *ACS Nano* **2022**, *16*, 19293.
- [142] L. Zhang, M. Fairbanks, T. L. Andrew, *Adv. Funct. Mater.* **2017**, *27*, 1700415.
- [143] R. Sun, H.-B. Zhang, J. Liu, X. Xie, R. Yang, Y. Li, S. Hong, Z.-Z. Yu, *Adv. Funct. Mater.* **2017**, *27*, 1702807.
- [144] M. C. Vu, D. Mani, J.-B. Kim, T.-H. Jeong, S. Park, G. Murali, I. In, J.-C. Won, D. Losic, C.-S. Lim, S.-R. Kim, *Composites, Part A* **2021**, *149*, 106574.
- [145] X. Tang, J. Luo, Z. Hu, S. Lu, X. Liu, S. Li, X. Zhao, Z. Zhang, Q. Lan, P. Ma, Z. Wang, T. Liu, *Nano Res.* **2023**, *16*, 1755.
- [146] T. Yun, H. Kim, A. Iqbal, Y. S. Cho, G. S. Lee, M.-K. Kim, S. J. Kim, D. Kim, Y. Gogotsi, S. O. Kim, C. M. Koo, *Adv. Mater.* **2020**, *32*, 1906769.
- [147] Y. Liu, N. Wu, S. Zheng, Y. Yang, B. Li, W. Liu, J. Liu, Z. Zeng, *ACS Appl. Mater. Interfaces* **2022**, *14*, 50120.
- [148] L. Wang, L. Chen, P. Song, C. Liang, Y. Lu, H. Qiu, Y. Zhang, J. Kong, J. Gu, *Composites, Part B* **2019**, *171*, 111.
- [149] X. Jin, J. Wang, L. Dai, X. Liu, L. Li, Y. Yang, Y. Cao, W. Wang, H. Wu, S. Guo, *Chem. Eng. J.* **2020**, *380*, 122475.
- [150] S.-J. Wang, D.-S. Li, L. Jiang, *Adv. Mater. Interfaces* **2019**, *6*, 1900961.
- [151] L. Liang, G. Han, Y. Li, B. Zhao, B. Zhou, Y. Feng, J. Ma, Y. Wang, R. Zhang, C. Liu, *ACS Appl. Mater. Interfaces* **2019**, *11*, 25399.
- [152] N. Wu, B. Li, F. Pan, R. Zhang, J. Liu, Z. Zeng, *Sci. China Mater.* **2023**, *66*, 1597.
- [153] M. Han, C. E. Shuck, A. Singh, Y. Yang, A. C. Foucher, A. Goad, B. McBride, S. J. May, V. B. Shenoy, E. A. Stach, Y. Gogotsi, *Cell. Rep.* **2022**, *3*, 101073.



Filipa M. Oliveira obtained her Ph.D. in 2020 in advanced materials and processing from the University of Minho, Portugal, with a thesis focused on polyamide 6 composites with tailored conductivity, dielectric, and electromagnetically shielding properties. She then moved to the University of Chemistry and Technology Prague, Czech Republic, to become a postdoctoral researcher. She is interested in 2D materials and their composites, and recently started a Chemfells Individual Fellowship to work on 2D materials for electromagnetic shielding applications.



Jalal Azadmanjiri received his Ph.D. in materials science and engineering from Monash University, Melbourne, Australia followed by a postdoctoral research fellowship at the Swinburne University of Technology. Recently he succeeded to get CZ Marie Curie (Chemfells IV) fellowship to work on 2D nanomaterials, their synthesis, characterization, and applications. His research interests include nanomaterials and nanotechnology, focusing on the design, synthesis, functionalization, and characterization of nanomaterials in 0D, 1D, and 2D structures. He is also interested in the development of hybrid materials with layered nanostructures for energy storage and energy conversion applications, and the study of their surfaces and interfaces.



Xuehang Wang is an assistant professor in the Department of Radiation Science and Technology at Delft University of Technology. She earned her Ph.D. in chemical engineering from the Norwegian University of Science and Technology in 2016 and was a postdoctoral researcher at A.J. Drexel Nanomaterials Institute, Drexel University from 2017 to 2020. Her research focuses on gaining an understanding of the charge mechanisms of energy storage devices, particularly the electrolyte transport at the electrode-electrolyte interfaces of 2D MXenes and various carbon materials.



Minghao Yu received his PhD degree in Material Physics and Chemistry from Sun Yat-sen University in June 2017. In March 2019, he became a research group leader of the Chair for Molecular Functional Materials at Technische Universität Dresden. His research interests focus on the development of advanced functional materials for applications of energy storage (supercapacitors and metal-ion batteries) and conversion (electrocatalysis and metal-air batteries).



Zdeněk Sofer is a full professor at the University of Chemistry and Technology Prague, Czech Republic, since 2019. He also received his Ph.D. from the University of Chemistry and Technology Prague in 2008. During his Ph.D., he spent one year at Forschungszentrum Jülich (Peter Grünberg Institute, Germany), followed by postdoctoral experience at the University of Duisburg-Essen, Germany. He works on semiconductors and 2D materials, their synthesis, crystal growth, chemical modifications, and functionalization as well as potential applications in the field of catalysis, energy storage and conversion, and optoelectronic and sensor systems.